Supplement of Geosci. Model Dev., 14, 5239–5268, 2021
https://doi.org/10.5194/gmd-14-5239-2021-supplement

Geoscientific Model Development
Open Access
EGU

Supplement of

Improvements to the representation of BVOC chemistry–climate interactions in UKCA (v11.5) with the CRI-Strat 2 mechanism: incorporation and evaluation

James Weber et al.

Correspondence to: James Weber (jmw240@cam.ac.uk)

Section S1

1.1 Updates to CS to produce CS2

CRI-STRAT (CS) reactions are shown in black, CRI-STRAT 2 (CS2) reactions in red. Pairings show a direct swap while struck-through black reactions indicate CS reactions which were removed with no direct replacement. Red reactions without a black partner reaction are new reactions to the CS2. For termolecular reactions, complex rate constants are used and in these cases the low pressure limit (k_0), high pressure limit (k_1) and F_C value are specified.

Termolecular Reactions

O(3P) + NO = NO2: $k_0 = 9 \times 10^{-32}[M](T/300)^{-1.5}$, $k_1 = 3 \times 10^{-11}$ $F_C = 0.6$

O(3P) + NO = NO2: $k_0 = 1 \times 10^{-31}[M](T/300)^{-1.6}$, $k_1 = 5 \times 10^{-11}(T/300)^{-0.3}$ $F_C = 0.85$

O(3P) + NO2 = NO3: $k_0 = 9 \times 10^{-32}[M](T/300)^{-2}$, $k_1 = 2.2 \times 10^{-11}$ $F_C = 0.6$

O(3P) + NO2 = NO3: $k_0 = 1.30 \times 10^{-31}[M](T/300)^{-1.5}$, $k_1 = 2.30 \times 10^{-11}(T/300)^{0.24}$ $F_C = 0.6$

HO2 + NO2 = HO2NO2: $k_0 = 1.80 \times 10^{-31}[M](T/300)^{-3.2}$, $k_1 = 4.70 \times 10^{-12}$ $F_C = 0.6$

HO2 + NO2 = HO2NO2: $k_0 = 1.40 \times 10^{-31}[M](T/300)^{-3.1}$, $k_1 = 4.00 \times 10^{-12}$ $F_C = 0.4$

OH + NO = HONO: $k_0 = 7.40 \times 10^{-31}[M](T/300)^{-2.4}$, $k_1 = 3.30 \times 10^{-11}(T/300)^{-0.3}$ $F_C = e^{-T/1420}$

OH + NO = HONO: $k_0 = 7.40 \times 10^{-31}[M](T/300)^{-2.4}$, $k_1 = 3.30 \times 10^{-11}(T/300)^{-0.3}$ $F_C = 0.81$

OH + NO2 = HONO2: $k_0 = 2.60 \times 10^{-30}[M](T/300)^{-3.2}$, $k_1 = 2.40 \times 10^{-11}(T/300)^{-1.3}$ $F_C = 0.6$

OH + NO2 = HONO2: $k_0 = 3.20 \times 10^{-30}[M](T/300)^{-4.5}$, $k_1 = 3.00 \times 10^{-11}$ $F_C = 0.41$

MeCO3 + NO2 = PAN: $k_0 = 8.50 \times 10^{-29}[M](T/300)^{-6.50}$, $k_1 = 1.10 \times 10^{-11}(T/300)^{-1.0}$ $F_C = 0.60$

MeCO3 + NO2 = PAN: $k_0 = 3.28 \times 10^{-28}[M](T/300)^{-6.87}$, $k_1 = 1.125 \times 10^{-11}(T/300)^{-1.105}$ $F_C = 0.30$

EtCO3 + NO2 = PPAN: $k_0 = 8.50 \times 10^{-29}[M](T/300)^{-6.50}$, $k_1 = 1.10 \times 10^{-11}(T/300)^{-1.0}$ $F_C = 0.60$

EtCO3 + NO2 = PPAN: $k_0 = 3.28 \times 10^{-28}[M](T/300)^{-6.87}$, $k_1 = 1.125 \times 10^{-11}(T/300)^{-1.105}$ $F_C = 0.30$

NO2 + NO3 = N2O5: $k_0 = 2.20 \times 10^{-30}[M](T/300)^{-3.90}$, $k_1 = 1.50 \times 10^{-12}(T/300)^{-0.7}$ $F_C = 0.60$

NO2 + NO3 = N2O5 : $k_0 = 3.60 \times 10^{-30}[M](T/300)^{-4.10}$, $k_1 = 1.90 \times 10^{-12}(T/300)^{-0.2}$ $F_C = 0.35$

HOCH2CO3 + NO2 = PHAN : $k_0 = 8.50 \times 10^{-29}[M](T/300)^{-6.50}$, $k_1 = 1.10 \times 10^{-11}(T/300)^{-1.0}$ $F_C = 0.60$

HOCH2CO3 + NO2 = PHAN : $k_0 = 3.28 \times 10^{-28}[M](T/300)^{-6.87}$, $k_1 = 1.125 \times 10^{-11}(T/300)^{-1.105}$ $F_C = 0.30$

RTN26O2 + NO2 = RTN26PAN : $k_0 = 6.14 \times 10^{-29}[M](T/300)^{-6.87}$, $k_1 = 7.94 \times 10^{-12}(T/300)^{-1.0}$ $F_C = 0.60$

RTN26O2 + NO2 = RTN26PAN : $k_0 = 2.368 \times 10^{-28}[M](T/300)^{-6.50}$, $k_1 = 8.123 \times 10^{-11}(T/300)^{-1.105}$ $F_C = 0.30$

~~RU12O2 + NO2 = RU12PAN~~ : $k_0 = 5.19 \times 10^{-30}[M](T/300)^{-6.50}$, $k_1 = 6.71 \times 10^{-13}(T/300)^{-1.00}$ $F_C = 0.60$

~~RU12PAN = RU12O2 + NO2~~ : $k_0 = 1.10 \times 10^{-5}[M]e^{-10100/T}$, $k_1 = 1.90 \times 10^{17}e^{-14100/T}$ $F_C = 0.30$

RU12O2 = DHCARB9 + CO + OH : $k = 2.40 \times 10^{5}e^{-5300/T}$

MACO3 + NO2 = MPAN : $k_0 = 3.28 \times 10^{-28}[M](T/300)^{-6.87}$, $k_1 = 1.125 \times 10^{-11}(T/300)^{-1.105}$ $F_C = 0.60$

MPAN = RU10O2 + NO2 : $k_0 = 1.105 \times 10^{-5}[M]e^{-10100/T}$, $k_1 = 1.90 \times 10^{17}e^{-14100/T}$ $F_C = 0.30$

MPAN = MACO3 + NO2 : $k = 1.60 \times 10^{16}e^{-13500/T}$

RU14O2 = 0.5DHPR12O2 + 0.5 HPUCARB12 + 0.5 HO2 : $k = 2.76 \times 10^{7}e^{-6597/T}$*

RU14O2 = UCARB10 + OH + CO: $k = 1.24 \times 10^{11}e^{-9570/T}$

DHPR12O2 = DHPCARB9 + CO + OH: $k = 3.0 \times 10^{7}e^{-5300/T}$

RU10AO2 = CARB7 + CO + OH: $k = 3.0 \times 10^{7}e^{-5300/T}$

*This reaction, along with 4 bimolecular reactions, allows the $k_{bulk1,6H}$ rate constant to be represented in the framework of UKCA.

Photolysis Reactions

CARB3 + PHOTON = CO + CO + HO2 + HO2 : 9.46*jhchoa
CARB3 + PHOTON = CO + CO + HO2 + HO2 : Glyxla from Prather et al (2013)
CARB3 + PHOTON = CO + CO + H2 : Glyxlb from Prather et al (2013)
CARB3 + PHOTON = HCHO + HO2 : Glyxlc from Prather et al (2013)

~~TNCARB12 + PHOTON = RN9O2 + HOCH2CO3 : 5.47e-4*jno2~~
~~TNCARB11 + PHOTON = RTN10O2 + CO + HO2 : 0.015*jno2~~

UCARB12 + PHOTON = MeCO3 + HOCH2CHO + CO + HO2 : jhchoa
UCARB12 + PHOTON = MeCO3 + HOCH2CHO + CO + HO2 : 0.25*jhchoa
UCARB12 + PHOTON = RU12O2 + HO2 : 0.5*jmacr
UCARB12 + PHOTON = CARB7 + CO + CO + HO2 + HO2 : 0.25*jmacr

NUCARB12 + PHOTON = NOA + CO + CO + HO2 : jmacr
NUCARB12 + PHOTON = HUCARB9 + CO + NO2 : 0.6066*jno2

NRU12OOH + PHOTON = NOA + CO + HO2 + OH: jmhp
NRU12OOH + PHOTON = NOA + CARB3 + HO2 + OH: jmhp

RU14NO3 + PHOTON = UCARB10 + HCHO + HO2 + NO2 : jiprn
RU12NO3 + PHOTON = CARB6 + HOCH2CHO + HO2 + NO2 : 7.583e-3*jno2
RU10NO3 + PHOTON = MeCO3 + HOCH2CHO + NO2 : 1.213e-3*jno2

HPUCARB12 + PHOTON = HUCARB9 + CO + OH + OH : 91.65*jmacr
HPUCARB12 + PHOTON = CARB7 + CO + CO + HO2 + OH : 91.65*jmacr
HUCARB9 + PHOTON = CARB6 + CO + HO2 + OH : 91.65*jmacr

DHPR12OOH + PHOTON = DHPCARB9 + CO + OH + HO2 : jetcho
DHPR12OOH + PHOTON = CARB3 + RN8OOH + OH + OH : 3*jmhp

DHCARB9 + PHOTON = CARB7 + CO + HO2 + HO2 : jetcho

NUCARB12 + PHOTON = CARB7 + CO + CO + HO2 + NO2 : 6.066e-3*jno2

Bimolecular Reactions

A significant number of the RO_2 + NO and RO_2 + NO_3 reactions changed only in their rate constants (rate constant changes shown below) and these changes are not listed here. Where the reactions changed in the branching ratio and/or products, the reactions are shown.

CS: $k_{APNO} = 8.1 \times 10^{-12} e^{290/T}$
CRI v2.2 $k_{APNO} = 7.5 \times 10^{-12} e^{290/T}$

CS: $k_{RO2+NO} = 2.4 \times 10^{-12} e^{360/T}$
CRI v2.2 $k_{RO2+NO} = 2.7 \times 10^{-12} e^{360/T}$

CS: $k_{RO2+NO_3} = 2.5 \times 10^{-12}$
CRI v2.2 $k_{RO2+NO_3} = 2.3 \times 10^{-12}$

O(1D) + H2O = OH + OH : $k = 2.20 \times 10^{-10}$ cm^3 $molecules^{-1}$ s^{-1}
O(1D) + H2O = OH + OH : $k = 2.14 \times 10^{-10}$ cm^3 $molecules^{-1}$ s^{-1}

O(1D) + N2 = OH + OH : $k = 1.80 \times 10^{-10} e^{110/T}$ cm^3 $molecules^{-1}$ s^{-1}
O(1D) + N2 = OH + OH : $k = 2.00 \times 10^{-11} e^{130/T}$ cm^3 $molecules^{-1}$ s^{-1}

O(1D) + O2 = OH + OH : $k = 3.20 \times 10^{-11} e^{70/T}$ cm^3 $molecules^{-1}$ s^{-1}
O(1D) + O2 = OH + OH : $k = 3.20 \times 10^{-11} e^{67/T}$ cm^3 $molecules^{-1}$ s^{-1}

HO2 + NO = OH + NO2 : $k = 3.60 \times 10^{-12}\, e^{270/T}$
HO2 + NO = OH + NO2 : $k = 3.45 \times 10^{-12}\, e^{270/T}$

OH + HO2NO2 = H2O + NO2 + O2 : $k = 1.90 \times 10^{-12}\, e^{270/T}$
OH + HO2NO2 = H2O + NO2 + O2 : $k = 3.20 \times 10^{-13}\, e^{690/T}$

OH + PAN = HCHO + CO + NO2 : $k = 9.50 \times 10^{-13} e^{-650/T}$
OH + PAN = HCHO + CO + NO2 : $k = 3.40 \times 10^{-14}$

OH + MPAN = CARB7 + CO + NO2 : $k = 3.60 \times 10^{-12}$
OH + MPAN = CARB7 + CO + NO2 : $k = 6.38 \times 10^{-12}$

OH + MeONO2 = HCHO + NO2 + H2O: $k = 1.00 \times 10^{-14} e^{-1060/T}$
OH + MeONO2 = HCHO + NO2 + H2O: $k = 4.00 \times 10^{-13} e^{-845/T}$

MeOO + NO = HCHO + NO2 + HO2: $k = 3.00 \times 10^{-12} e^{-280/T}$
MeOO + NO = HCHO + NO2 + HO2: $k = 2.298 \times 10^{-12} e^{-360/T}$

MeOO + NO = MeONO2 : $k = 3.00 \times 10^{-15} e^{-280/T}$
MeOO + NO = MeONO2 : $k = 2.30 \times 10^{-15} e^{-360/T}$

MeOO + NO = HO2 + HCHO + NO2 : $k = 1.00 \times 10^{-12}$
MeOO + NO3 = HO2 + HCHO + NO2 : $k = 1.20 \times 10^{-12}$

NO3 + C5H8 = NRU14O2 : $k = 3.0 \times 10^{-12} e^{-466/T}$
NO3 + C5H8 = NRU14O2 : $k = 3.15 \times 10^{-12} e^{-450/T}$

O3 + C5H8 = UCARB10 + CO + HO2 + OH : $k = 2.12 \times 10^{-15} e^{-1913/T}$
O3 + C5H8 = UCARB10 + HCOOH : $k = 5.74 \times 10^{-15} e^{-1913/T}$
O3 + C5H8 = UCARB10 + CO + HO2 + OH : $k = 1.288 \times 10^{-15} e^{-1995/T}$
O3 + C5H8 = HCHO + MeOO + CO + HO2 : $k = 9.79 \times 10^{-16} e^{-1995/T}$
O3 + C5H8 = UCARB10 + HCOOH : $k = 1.80 \times 10^{-15} e^{-1995/T}$
O3 + C5H8 = UCARB10 + HCHO + H2O2 : $k = 3.97 \times 10^{-15} e^{-1995/T}$
O3 + C5H8 = MeCO3 + HCHO + CO + OH : $k = 1.29 \times 10^{-15} e^{-1995/T}$
O3 + C5H8 = UCARB10 + CO : $k = 9.785 \times 10^{-16} e^{-1995/T}$

OH + C5H8 = RU14O2 : $k = 2.54 \times 10^{-12} e^{410/T}$
OH + C5H8 = RU14O2 : $k = 2.70 \times 10^{-12} e^{390/T}$

OH + UCARB10 = RU10O2 : $k = 2.50 \times 10^{-11}$
OH + UCARB10 = RU10O2 : $k = 3.84 \times 10^{-12} e^{533/T}$

NO3 + UCARB10 = RU10O2 + HONO2 : $k = 1.44 \times 10^{-12}\, e^{-1862/T}$
NO3 + UCARB10 = RU10O2 + HONO2: $k = 5.98 \times 10^{-13}\, e^{-1862/T}$

O3 + UCARB10 = HCHO + MeCO3 + CO + OH : $k = 1.68 \times 10^{-18}$
O3 + UCARB10 = HCHO + MeCO3 + CO + OH : $k = 3.84 \times 10^{-16} e^{-1710/T}$

O3 + UCARB10 = HCHO + CARB6 + H2O2 : $k = 1.17 \times 10^{-18}$
O3 + UCARB10 = HCHO + CARB6 : $k = 8.16 \times 10^{-16} e^{-1710/T}$

OH + UCARB12 = RU10O2 : $k = 4.52 \times 10^{-11}$
OH + UCARB12 = RU10O2 : $k = 6.42 \times 10^{-11}$

NO3 + UCARB12 = RU10O2 : $k = 4.52 \times 10^{-11}$

NO3 + UCARB12 = RU10O2 : $k = 6.42 \times 10^{-11}$

O3 + UCARB12 = HOCH2CHO + MeCO3 + CO + OH : $k = 2.14 \times 10^{-17}$
O3 + UCARB12 = HOCH2CHO + MeCO3 + CARB3 + OH : $k = 6.00 \times 10^{-18}$

O3 + UCARB12 = HOCH2CHO + CARB6 + H2O2 : $k = 2.64 \times 10^{-18}$
O3 + UCARB12 = CARB6 + CO + OH + HO2 : $k = 1.20 \times 10^{-17}$

OH + RU14OOH = UCARB12 + OH: $k = 7.51 \times 10^{-11}$
OH + RU14OOH = 0.09UCARB12 + 0.94OH + 0.85IEPOX + 0.06RU14O2: $k = 7.14 \times 10^{-11}$

OH + RU12OOH = RU12O2: $k = 3.00 \times 10^{-11}$
OH + RU12OOH = RU10OOH + CO + HO2: $k = 3.50 \times 10^{-11}$

OH + RU10OOH = RU10O2: $k = 3.00 \times 10^{-11}$
OH + RU10OOH = CARB7 + CO + OH: $k = 3.84 \times 10^{-11}$

MPAN + OH = HMML + NO3: $k = 2.262 \times 10^{-11}$

RU10O2 + NO3 = CARB7 + HCHO + HO2 + NO2 : $k = 5.00 \times 10^{-13}$
RU10AO2 + NO3 = CARB7 + HCHO + HO2 + NO2 : $k = 2.30 \times 10^{-12}$

RU10O2 + RO2 = CARB7 + HCHO + HO2 : $k = 4.00 \times 10^{-13}$
RU10AO2 + RO2 = CARB7 + CO + HO2 : $k = 3.60 \times 10^{-13}$

RU10AO2 + NO = CARB7 + CO + HO2 : $k = 2.665 \times 10^{-12} e^{360/T}$

RU10AO2 + HO2 = RU10OOH + CO + HO2 : $k = 1.819 \times 10^{-13} e^{1300/T}$

OH + CARB3 = CO + OH : $k = 6.2 \times 10^{-13} e^{340/T}$

DHPR12O2 + NO = CARB3 + RN8OOH + OH + NO2 : $k = 2.70 \times 10^{-12} e^{360/T}$;
DHPR12O2 + NO3 = CARB3 + RN8OOH + OH + NO2 : $k = 2.30 \times 10^{-12}$;
DHPR12O2 + HO2 = DHPR12OOH : $k = 2.91 \times 10^{-13} e^{1300/T}$ *0.706 ;
DHPR12O2 + RO2 = CARB3 + RN8OOH + OH : $k = 7.60 \times 10^{-13}$;

OH + HUCARB9 = CARB6 + CO + HO2 : $k = 5.78 \times 10^{-11}$;

OH + DHCARB9 = CARB6 + HO2 : $k = 3.42 \times 10^{-11}$;

OH + DHPCARB9 = RN8OOH + CO + OH : $k = 3.64 \times 10^{-11}$

RU12O2 + NO = CARB7 + HOCH2CO3 + NO2 : $k = 4.59 \times 10^{-13} e^{360/T}$
RU12O2 + NO3 = CARB7 + HOCH2CO3 + NO2 : $k = 4.05 \times 10^{-13}$

OH + IEPOX = RU12O2 : $k = 1.16 \times 10^{-11}$

OH + HMML = CARB6 + OH : $k = 4.33 \times 10^{-12}$*0.7 ;
OH + HMML = HCOOH + CH3CO3 : $k = 4.33 \times 10^{-12}$*0.3 ;
OH + DHPR12OOH = DHPCARB9 + CO + OH : $k = 5.64 \times 10^{-11}$;
OH + RU12NO3 = CARB7 + CARB3 + NO2 : $k = 2.50 \times 10^{-12}$;
OH + RU10NO3 = CARB7 + CO + NO2 : $k = 5.26 \times 10^{-13}$;

RU10AO2 + NO = RU10NO3 : $k = 2.70 \times 10^{-12} e^{360/T}$ *0.013 ;
RU10AO2 + NO = CARB7 + CO + HO2 + NO2 : $k = 2.70 \times 10^{-12} e^{360/T}$ *0.987 ;
RU10AO2 + NO3 = CARB7 + CO + HO2 + NO2 : $k = 2.30 \times 10^{-12}$;

RU10AO2 + HO2 = RU10OOH : $k = 2.91 \times 10^{-13} e^{1300/T}$ *0.625 ;
RU10AO2 + RO2= CARB7 + CO + HO2 : $k = 3.60 \times 10^{-13}$

MACO3 + NO = CH3O2 + CO + HCHO + HO2 + NO2 : $k = 7.50 \times 10^{-12} e^{290/T}$ *0.65 ;
MACO3 + NO = CH3CO3 + HCHO + HO2 + NO2 : $k = 7.50 \times 10^{-12} e^{290/T}$ *0.35 ;
MACO3 + NO3 = CH3O2 + CO + HCHO + HO2 + NO2 : $k = 2.30 \times 10^{-12}$*1.74*0.65 ;
MACO3 + NO3 = CH3CO3 + HCHO + HO2 + NO2 : $k = 2.30 \times 10^{-12}$*1.74*0.35 ;
MACO3 + HO2 = RU10OOH : $k = 5.20 \times 10^{-13} e^{980/T}$ *0.56 ;
MACO3 + HO2 = CH3O2 + CO + HCHO + OH : $k = 5.20 \times 10^{-13} e^{980/T}$ *0.44 ;

OH + HPUCARB12 = HUCARB9 + CO + OH : $k = 5.20 \times 10^{-11}$;
O3 + HPUCARB12 = CARB3 + CARB6 + OH + OH : $k = 2.4 \times 10^{-17}$;
NO3 + HPUCARB12 = HUCARB9 + CO + OH + HNO3 : $k = 1.44 \times 10^{-12} e^{-1862/T}$ * 4.25 ;

NRU12O2 + NO = NOA + CARB3 + HO2 + NO2 : $k = 1.35 \times 10^{-12} e^{360/T}$
NRU12O2 + NO3 = NO3 + CARB3 + HO2 + NO2 : $k = 1.15 \times 10^{-12}$;
NRU12O2 + RO2 = NOA + CARB3 + HO2 + NO2 : $k = 4.80 \times 10^{-13}$;
RU12O2 + RO2 = CARB7 + HOCH2CO3 : $k = 7.392 \times 10^{-14}$
HOCH2CO3 + HO2 = HCHO + HO2 + OH : $k = 2.288 \times 10^{-13} e^{980/T}$

RU14NO3 + OH = RU12NO3 + HO2 : $k = 5.40 \times 10^{-12}$
RU14NO3 + OH = RU10NO3 + HCHO + HO2 : $k = 1.44 \times 10^{-11}$

*RU14O2 + NO = 0.5HPUCARB12 + 0.5HO2 + 0.5DHPR12O2 + NO : $k = 1.399 \times 10^{-15} e^{1668/T}$
*RU14O2 + NO3 = 0.5HPUCARB12 + 0.5HO2 + 0.5DHPR12O2 + NO3: $k = 1.191 \times 10^{-15} e^{1308/T}$
*RU14O2 + HO2 = 0.5HPUCARB12 + 0.5HO2 + 0.5DHPR12O2 + HO2 : $k = 1.064 \times 10^{-15} e^{2608/T}$
*RU14O2 + RO2 = 0.5HPUCARB12 + 0.5HO2 + 0.5DHPR12O2 + RO2 : $k = 6.527 \times 10^{-16} e^{1308/T}$

*These reactions, when combined with the unimolecular reaction RU14O2 = 0.5HPUCARB12 + 0.5HO2 + 0.5DHPR12O2, represents the $k_{bulk1,6H}$ rate constant in the framework of UKCA.
EtOO + NO = MeCHO + HO2 + NO2: $k = 2.58 \times 10^{-12} e^{365/T}$
EtOO + NO = RU10NO3 + HCHO + HO2 : $k = 2.53 \times 10^{-12} e^{380/T}$

EtCO3 + HO2 = EtCO3H : $k = 4.40 \times 10^{-13} e^{980/T}$
EtCO3 + HO2 = EtCO3H + HCHO + HO2 : $k = 4.30 \times 10^{-13} e^{1040/T}$

EtOO + HO2 = EtOOH : $k = 7.50 \times 10^{-13} e^{700/T}$
EtOO + HO2 = EtOOH : $k = 4.30 \times 10^{-13} e^{870/T}$

MeCO3 + HO2 = MeCO3H : $k = 4.31 \times 10^{-13} e^{1040/T}$
MeCO3 + HO2 = MeCO3H : $k = 2.91 \times 10^{-13} e^{980/T}$

MeCO3 + HO2 = MeOO + OH : $k = 2.29 \times 10^{-13} e^{980/T}$

NO + HO2 = NO2 + OH : $k = 3.60 \times 10^{-12} e^{270/T}$
NO + HO2 = NO2 + OH : $k = 3.45 \times 10^{-12} e^{270/T}$

MeOO + NO = HCHO + HO2 + NO2 : $k = 3.00 \times 10^{-12} e^{280/T}$
MeOO + NO = HCHO + HO2 + NO2 : $k = 2.298 \times 10^{-13} e^{360/T}$

MeOO + NO = MeONO2 : $k = 3.00 \times 10^{-15} e^{280/T}$
MeOO + NO = MeONO2 : $k = 2.30 \times 10^{-15} e^{360/T}$

MeOO + NO3 = HO2 + HCHO + NO2 : $k = 1.00 \times 10^{-12}$
MeOO + NO3 = HO2 + HCHO + NO2 : $k = 1.20 \times 10^{-12}$

HCHO + NO3 = HONO2 + HO2 + CO : $k = 5.80 \times 10^{-16}$

HCHO + NO3 = HONO2 + HO2 + CO : $k = 5.50 \times 10^{-16}$

MeCHO + NO3 = HONO2 + HO2 + CO : $k = 1.44 \times 10^{-12} e^{-1862/T}$

MeCHO + NO3 = HONO2 + HO2 + CO : $k = 1.40 \times 10^{-12} e^{-1860/T}$

EtCHO + OH = H2O + EtCO3 : $k = 1.96 \times 10^{-11}$

EtCHO + OH = H2O + EtCO3 : $k = 4.90 \times 10^{-12}$

MeCHO + OH = H2O + MeCO3 : $k = 5.55 \times 10^{-12} e^{311/T}$

MeCHO + OH = H2O + MeCO3 : $k = 4.70 \times 10^{-12} e^{345/T}$

MeOOH + OH = H2O + HCHO + OH : $k = 1.02 \times 10^{-12} e^{190/T}$

MeOOH + OH = H2O + HCHO + OH : $k = 2.12 \times 10^{-12} e^{190/T}$

O3 + C2H4 = H2O + HCHO + OH : $k = 1.19 \times 10^{-15} e^{-2580/T}$

O3 + C2H4 = H2O + HCHO + OH : $k = 1.18 \times 10^{-15} e^{-2850/T}$

O3 + C2H4 = HCHO + HCOOH : $k = 7.95 \times 10^{-15} e^{-2580/T}$

O3 + C2H4 = HCHO + HCOOH : $k = 7.91 \times 10^{-15} e^{-2850/T}$

NO3 + C2H4 = NRN6O2 : $k = 2.10 \times 10^{-16}$

NO3 + C2H4 = NRN9O2: $k = 3.30 \times 10^{-12} e^{-2880/T}$

OH + TOLUENE = AROH17 + HO2 : $k = 3.26 \times 10^{-13} e^{338/T}$

OH + TOLUENE = AROH17 + HO2 : $k = 3.24 \times 10^{-12} e^{340/T}$

OH + TOLUENE = RA16O2 : $k = 1.48 \times 10^{-12} e^{338/T}$

OH + TOLUENE = RA16O2 : $k = 1.48 \times 10^{-12} e^{340/T}$

NO3 + APINENE = NRTN28O2 : $k = 1.19 \times 10^{-12} e^{490/T}$

NO3 + APINENE = NRTN28O2 : $k = 1.20 \times 10^{-12} e^{490/T}$

O3 + APINENE = OH + Me2CO + RN18AO2 : $k = 8.08 \times 10^{-16} e^{-732/T}$

O3 + APINENE = OH + Me2CO + RN18AO2 : $k = 6.44 \times 10^{-16} e^{-644/T}$

O3 + APINENE = TNCARB26 + H2O2 : $k = 7.57 \times 10^{-17} e^{-732/T}$

O3 + APINENE = TNCARB26 + H2O2 : $k = 1.41 \times 10^{-16} e^{-644/T}$

O3 + APINENE = RCOOH25 : $k = 1.26 \times 10^{-16} e^{-732/T}$

O3 + APINENE = RCOOH25 : $k = 2.01 \times 10^{-17} e^{-644/T}$

O3 + BPINENE = RTX24O2 + OH : $k = 5.25 \times 10^{-18}$

O3 + BPINENE = RTX24O2 + OH : $k = 4.73 \times 10^{-16} e^{-1270/T}$

O3 + BPINENE = HCHO + TXCARB24 + H2O2 : $k = 3.00 \times 10^{-18}$

O3 + BPINENE = HCHO + TXCARB24 + H2O2 : $k = 2.70 \times 10^{-16} e^{-1270/T}$

O3 + BPINENE = HCHO + TXCARB22 : $k = 3.75 \times 10^{-18}$

O3 + BPINENE = HCHO + TXCARB22 : $k = 3.38 \times 10^{-16} e^{-1270/T}$

O3 + BPINENE = CO + TXCARB24 : $k = 3.00 \times 10^{-18}$

O3 + BPINENE = CO + TXCARB24 : $k = 2.70 \times 10^{-16} e^{-1270/T}$

OH + BENZENE = RA13O2 : $k = 1.10 \times 10^{-12} e^{-193/T}$

OH + BENZENE = RA13O2 : $k = 1.08 \times 10^{-12} e^{-190/T}$

342 OH + BENZENE = AROH14 + HO2 : $k = 1.23 \times 10^{-12} e^{-193/T}$
343 OH + BENZENE = AROH14 + HO2: $k = 1.22 \times 10^{-12} e^{-190/T}$
344
345
346 OH + n-PrOH = EtCHO + HO2 : $k = 2.71 \times 10^{-12}$
347 OH + n-PrOH = EtCHO + HO2: $k = 2.27 \times 10^{-12} e^{70/T}$
348
349 OH + n-PrOH = RN9O2 : $k = 2.82 \times 10^{-12}$
350 OH + n-PrOH = RN9O2 : $k = 2.33 \times 10^{-12} e^{70/T}$
351
352 RU10O2 + NO3 = CARB7 + HCHO + HO2 + NO2 : $k = 5.00 \times 10^{-13}$
353 RU10AO2 + NO3 = CARB7 + HO2 + CO + NO2 : $k = 2.30 \times 10^{-13}$
354
355 HOCH2CO3 + HO2 = HOCH2CO3H : $k = 4.30 \times 10^{-13} e^{1040/T}$
356 HOCH2CO3 + HO2 = HOCH2CO3H : $k = 2.912 \times 10^{-13} e^{980/T}$
357
358 NRU14O2 + HO2 = NRU14OOH : $k = 2.24 \times 10^{-13} e^{1300/T}$
359 NRU14O2 + HO2 = NRU14OOH : $k = 2.05 \times 10^{-13} e^{1300/T}$
360
361 NRU12O2 + HO2 = NRU12OOH : $k = 1.82 \times 10^{-13} e^{1300/T}$
362 NRU12O2 + HO2 = NRU12OOH : $k = 2.05 \times 10^{-13} e^{1300/T}$
363
364 RTN26O2 + HO2 = RTN26OOH : $k = 2.66 \times 10^{-13} e^{1300/T}$
365 RTN26O2 + HO2 = 0.56RTN26OOH + 0.44RTN25O2 + 0.44OH : $k = 5.20 \times 10^{-13} e^{980/T}$
366
367 CH3O2 + RO2 = HCHO + HO2 : $k = 6.01 \times 10^{-14} e^{416/T}$
368 CH3O2 + RO2 = HCHO : $k = 6.01 \times 10^{-14} e^{416/T}$
369 CH3O2 + RO2 = MeOH : $k = 6.01 \times 10^{-14} e^{416/T}$
370
371 $k_{CH3O2} = 1.03 \times 10^{-13} e^{365/T}$
372 CH3O2 + RO2 = HCHO + HO2 : $2*k_{CH3O2}*7.18*e^{-885/T}$
373 CH3O2 + RO2 = HCHO : $2*k_{CH3O2}*0.5*(1-7.18*e^{-885/T})$
374 CH3O2 + RO2 = CH3OH : $2*k_{CH3O2}*0.5*(1-7.18*e^{-885/T})$;
375
376 RU14O2 + HO2 = RU14OOH : $k = 2.24 \times 10^{-13} e^{1300/T}$
377 RU14O2 + HO2 = RU14OOH : $k = 2.05 \times 10^{-13} e^{1300/T}$
378
379 RU14O2 + RO2 = UCARB12 + HO2 : $k = 4.31 \times 10^{-13}$
380 RU14O2 + RO2 = UCARB12 + HO2 : $k = 1.26 \times 10^{-13}$
381
382 RU14O2 + RO2 = UCARB10 + HCHO + HO2 : $k = 1.28 \times 10^{-12}$
383 RU14O2 + RO2 = UCARB10 + HCHO + HO2 : $k = 1.13 \times 10^{-12}$
384
385 RU12O2 + RO2 = MeCO3 + HOCH2CHO : $k = 1.40 \times 10^{-12}$
386 RU12O2 + RO2 = MeCO3 + HOCH2CHO : $k = 1.772 \times 10^{-13}$
387
388 RU12O2 + RO2 = HO2 + CARB7 + CARB3 : $k = 6.00 \times 10^{-13}$
389 RU12O2 + RO2 = HO2 + CARB7 + CARB3 : $k = 1.668 \times 10^{-13}$
390
391 RU10O2 + RO2 = MeCO3 + HOCH2CHO : $k = 1.00 \times 10^{-12}$
392 RU10O2 + RO2 = MeCO3 + HOCH2CHO : $k = 1.28 \times 10^{-13}$
393
394 RU10O2 + RO2 = CARB6 + HCHO + HO2 : $k = 6.00 \times 10^{-13}$
395 RU10O2 + RO2 = CARB6 + HCHO + HO2 : $k = 5.49 \times 10^{-13}$
396
397 RU10O2 + RO2 = CARB7 + CO + HO2 : $k = 4.00 \times 10^{-13}$
398 RU10AO2 + RO2 = CARB7 + CO + HO2 : $k = 3.60 \times 10^{-13}$

NRU12O2 + RO2 = NOA + CO + HO2 : $k = 9.60 \times 10^{-13}$

NRU12O2 + RO2 = NOA + CO + HO2 : $k = 4.80 \times 10^{-13}$

RTN26O2 + RO2 = RTN25O2 : $k = 2.00 \times 10^{-12}$

RTN26O2 + RO2 = RTN25O2 : $k = 1.00 \times 10^{-11}$

RTN26O2 + RO2 = RTN25O2 : $k = 2.00 \times 10^{-12}$

RTN26O2 + RO2 = RTN25O2 : $k = 1.00 \times 10^{-11}$

OH + CARB3 = CO + CO + HO2 : $k = 1.14 \times 10^{-11}$

OH + CARB3 = CO + CO + HO2 : $k = 2.48 \times 10^{-12}$

OH + CARB6 = MeCO3 + CO : $k = 1.72 \times 10^{-11}$

OH + CARB6 = CO + CO + HO2 : $k = 1.90 \times 10^{-12} e^{575/T}$

OH + NOA = CARB6 + NO2 : $k = 1.30 \times 10^{-13}$

OH + NOA = CARB6 + NO2 : $k = 6.70 \times 10^{-13}$

OH + RU14NO3 = UCARB12 + NO2 : $k = 5.55 \times 10^{-11}$

OH + RU14NO3 = UCARB12 + NO2 : $k = 1.02 \times 10^{-11}$

OH + RN8OOH = CARB6 + OH : $k = 4.42 \times 10^{-12}$

OH + RN8OOH = CARB6 + OH : $k = 1.02 \times 10^{-11}$

RTN23O2 + NO = RTN23NO3 : $k = 2.83 \times 10^{-13} e^{360/T}$

RU12O2 + NO = RN12NO3 : $k = 9.45 \times 10^{-14} e^{360/T}$

~~RTN23O2 + OH = Me2CO + TNCARB12 + NO2 : $k = 5.37 \times 10^{-12}$~~

~~TNCARB12 + OH = TNCARB11 + HO2 : $k = 3.22 \times 10^{-12}$~~

~~TNCARB11 + OH = RTN10O2 + HO2 : $k = 1.33 \times 10^{-11}$~~

~~TNCARB11 + NO3 = RTN10O2 + CO + HONO2 : $k = 7.92 \times 10^{-12} e^{-1862/T}$~~

Wet Deposition Parameters

Table S1 - New or updated wet deposition parameters. Text/figures in parentheses show values used in CRI-STRAT (Archer-Nicholls et al., 2021)

Species	Surrogate	Reference	k(298K)	$-\Delta H/R$
HOC2H4OOH	HOC2H4OOH (EtOOH)	Schwantes et al (2020)	1.9e6 (3.4e2)	6.01e3 (5.70e3)
CARB7	Hydroxyacetone (Hydroxyacetone)	Schwantes et al (2020)	1.46e3 (1.4e2)	6.01e3 (5.70e3)
CARB10	Hydroxyacetone (Hydroxyacetone)	Schwantes et al (2020)	1.46e3 (1.4e2)	6.01e3 (5.70e3)
CARB13	Hydroxyacetone (Hydroxyacetone)	Schwantes et al (2020)	1.46e3 (1.4e2)	6.01e3 (5.70e3)
CARB16	Hydroxyacetone (Hydroxyacetone)	Schwantes et al (2020)	1.46e3 (1.4e2)	6.01e3 (5.70e3)

CARB3	Glyoxal (Methylglyoxal)	Schwantes et al (2020)	4.19e5 (3.5e3)	7.48e3 (7.2e3)
RA13NO3	RU14NO3 (no wet dep before)	Schwantes et al (2020)	8.34e3 (N/A)	6.01e3 (N/A)
RA16NO3	RU14NO3 (no wet dep before)	Schwantes et al (2020)	8.34e3 (N/A)	6.01e3 (N/A)
RA19NO3	RU14NO3 (no wet dep before)	Schwantes et al (2020)	8.34e3 (N/A)	6.01e3 (N/A)
RN8OOH	Hydroperoxy acetone (EtOOH)	Schwantes et al (2020)	1.16e4 (3.4e2)	6.01e3 (5.70e3)
RN11OOH	Hydroperoxy acetone (EtOOH)	Schwantes et al (2020)	1.16e4 (3.4e2)	6.01e3 (5.70e3)
RN14OOH	Hydroperoxy acetone (EtOOH)	Schwantes et al (2020)	1.16e4 (3.4e2)	6.01e3 (5.70e3)
RN17OOH	Hydroperoxy acetone (EtOOH)	Schwantes et al (2020)	1.16e4 (3.4e2)	6.01e3 (5.70e3)
RU14OOH	RU14OOH (EtOOH)	Schwantes et al (2020)	3.5e6 (3.4e2)	6.01e3 (5.70e3)
RU12OOH	MVKOOH (EtOOH)	Schwantes et al (2020)	1.24e6 (3.4e2)	6.01e3 (5.70e3)
RU10OOH	MVKOOH (EtOOH)	Schwantes et al (2020)	1.24e6 (3.4e2)	6.01e3 (5.70e3)
NRU14OOH	ISOPNOOH (EtOOH)	Schwantes et al (2020)	8.75e4 (3.4e2)	6.01e3 (5.70e3)
NRU12OOH	MVKN (EtOOH)	Schwantes et al (2020)	1.84e5 (3.4e2)	6.01e3 (5.70e3)
RN9OOH	HOC3H7OOH (EtOOH)	Schwantes et al (2020)	1.5e6 (3.4e2)	6.01e3 (5.70e3)
RA13OOH	BENZOOH (EtOOH)	Schwantes et al (2020)	2.3e3 (3.4e2)	6.01e3 (5.70e3)
RA16OOH	BENZOOH (EtOOH)	Schwantes et al (2020)	2.3e3 (3.4e2)	6.01e3 (5.70e3)
RA19OOH	BENZOOH (EtOOH)	Schwantes et al (2020)	2.3e3 (3.4e2)	6.01e3 (5.70e3)
RTN28OOH	Hydroperoxy	Schwantes et al	1.16e4 (3.4e2)	6.01e3 (5.70e3)

	acetone (EtOOH)	(2020)		
RTN26OOH	Hydroperoxy acetone (EtOOH)	Schwantes et al (2020)	1.16e4 (3.4e2)	6.01e3 (5.70e3)
RTN25OOH	Hydroperoxy acetone (EtOOH)	Schwantes et al (2020)	1.16e4 (3.4e2)	6.01e3 (5.70e3)
RTN14OOH	Hydroperoxy acetone (EtOOH)	Schwantes et al (2020)	1.16e4 (3.4e2)	6.01e3 (5.70e3)
RTX28OOH	Hydroperoxy acetone (EtOOH)	Schwantes et al (2020)	1.16e4 (3.4e2)	6.01e3 (5.70e3)
RTX24OOH	Hydroperoxy acetone (EtOOH)	Schwantes et al (2020)	1.16e5 (3.4e2)	6.01e3 (5.70e3)
RTX28OOH	Hydroperoxy acetone (EtOOH)	Schwantes et al (2020)	1.16e4 (3.4e2)	6.01e3 (5.70e3)
RTN26PAN	TERPA2PAN (no wet dep before)	Schwantes et al (2020)	9.59e3 (N/A)	6.01e3 (N/A)
RTN23NO3	Beta Isoprene hydroxy nitrate (no wet dep before)	Schwantes et al (2020)	8.34e3 (N/A)	6.01e3 (N/A)
RN9NO3	HONITR (no wet dep before)	Schwantes et al (2020)	2.64e3 (N/A)	6.01e3 (N/A)
RN12NO3	HONITR (no wet dep before)	Schwantes et al (2020)	2.64e3 (N/A)	6.01e3 (N/A)
RN15NO3	HONITR (no wet dep before)	Schwantes et al (2020)	2.64e3 (N/A)	6.01e3 (N/A)
RN18NO3	HONITR (no wet dep before)	Schwantes et al (2020)	2.64e3 (N/A)	6.01e3 (N/A)
RU14NO3	Beta Isoprene hydroxy nitrate (no wet dep before)	Schwantes et al (2020)	8.34e3 (N/A)	6.01e3 (N/A)

RTN28NO3	Beta Isoprene hydroxy nitrate (no wet dep before)	Schwantes et al (2020)	8.34e3 (N/A)	6.01e3 (N/A)
RTN25NO3	Beta Isoprene hydroxy nitrate (no wet dep before)	Schwantes et al (2020)	8.34e3 (N/A)	6.01e3 (N/A)
RTX28NO3	Beta Isoprene hydroxy nitrate (no wet dep before)	Schwantes et al (2020)	8.34e3 (N/A)	6.01e3 (N/A)
RTX22NO3	Beta Isoprene hydroxy nitrate (no wet dep before)	Schwantes et al (2020)	8.34e3 (N/A)	6.01e3 (N/A)
AROH14	Phenol (MeOH)	Schwantes et al (2020)	2.84e3 (2.3e2)	2.70e3 (4.9e3)
ARNOH14	Nitrophenol (MeOH)	Guo and Brimblecombe (2007)	8.5e1 (2.3e2)	6.27e3 (4.9e3)
AROH17	Phenol (MeOH)	Schwantes et al (2020)	5.67e2 (2.3e2)	5.80e3 (4.9e3)
ARNOH17	Nitrophenol (MeOH)	Guo and Brimblecombe (2007)	8.5e1 (2.3e2)	6.27e3 (4.9e3)
IEPOX	IEPOX (new species)	Schwantes et al (2020)	3.0e7 (N/A)	6.01e3 (N/A)
HMML	HMML (new species)	Schwantes et al (2020)	2.3e5 (N/A)	6.01e3 (N/A)
HUCARB9	Unsaturated hydroxy carbonyl (new species)	Schwantes et al (2020)	1.1e5 (N/A)	6.00e3 (N/A)
HPUCARB12	HPALD (new species)	Schwantes et al (2020)	2.3e5 (N/A)	6.01e3 (N/A)
DHPCARB9	DHPMPAL (new species)	Schwantes et al (2020)	9.37e7 (N/A)	6.01e3 (N/A)
DHPR12OOH	DHPMPAL (new	Schwantes et al	9.37e7 (N/A)	6.01e3 (N/A)

	species)	(2020)		
DHCARB9	Hydroxy acetone (new species)	Schwantes et al (2020)	1.46e3 (N/A)	4.9e3 (N/A)
RU12NO3	MVKN (new species)	Schwantes et al (2020)	1.84e5 (N/A)	6.00e3 (N/A)
RU1NO3	MVKN (new species)	Schwantes et al (2020)	1.84e5 (N/A)	6.00e3 (N/A)

436
437
438
439 **Table S2 - Emitted species and their sources. All biogenic emissions are 2011-201 MEGAN-MACC**
440 **climatologies and oceanic emissions are POET 1990 emissions.**

Species	Source(s)
SO_2	Natural, anthropogenic (surface and high)
DMS	Natural, biomass burning
C_2H_4	Anthropogenic, biomass burning, biogenic, oceanic
C_2H_6	Anthropogenic, biomass burning, biogenic, oceanic
C_3H_6	Anthropogenic, biomass burning, biogenic, oceanic
C_3H_8	Anthropogenic, biomass burning, biogenic, oceanic
C_4H_{10}	Anthropogenic, biomass burning, biogenic, oceanic
C_5H_8	Biomass burning, biogenic
CO	Anthropogenic, biomass burning, biogenic, oceanic
EtCHO (propionaldehyde)	Anthropogenic, biomass burning, biogenic
EtOH	Anthropogenic, biomass burning, biogenic
HCHO	Anthropogenic, biomass burning, biogenic
HCOOH (methanoic acid)	Anthropogenic, biomass burning, biogenic
MEK (methyl ethyl ketone)	Anthropogenic, biomass burning, biogenic

Me_2CO (acetone)	Anthropogenic, biomass burning, biogenic
MeCHO (acetaldehyde)	Anthropogenic, biomass burning, biogenic
$MeCO_2H$ (ethanoic acid)	Anthropogenic, biomass burning, biogenic
MeOH (methanol)	Anthropogenic, biomass burning, biogenic
TBUT2ENE (trans but-2-ene)	Anthropogenic, biomass burning, biogenic
Toluene	Anthropogenic, biomass burning, biogenic
NO	Anthropogenic, biomass burning, biogenic, soil
NH_3	Anthropogenic, biomass burning, biogenic, oceanic
Alpha pinene	Biomass burning, biogenic
Beta pinene	Biomass burning, biogenic
Black Carbon	Biofuel, biomass burning (surface and high), fossil fuels
Benzene	Biomass burning, anthropogenic
C_2H_2	Biomass burning, anthropogenic
CH_4^*	Biomass burning
$HOCH_2CHO$	Biomass burning
Organic carbon	Biofuel, biomass burning (surface and high), fossil fuels
Toluene	Biogenic, anthropogenic, biomass burning
Oxylene	Anthropogenic, biomass burning

* Lower boundary condition imposed in model

For the observation-model comparisons, the CS and CS2 runs used anthropogenic timeseries emissions for all runs up to and including 2014 and 2014 timeslice emissions for the runs in 2016 due to a current lack of post-2014 emissions for CRI. All emissions were based on the CMIP6 CEDS inventories (Hosely et al. 2018). The ST runs used timeseries anthropogenic emissions based on the CMIP6 CEDS inventories for all runs up to 2014 and then time series emissions based on SSP370 for runs in 2016.

Section S2 Sensitivity Test Changes

CRI v2.2 reactions are shown in red, the changes made for each sensitivity test are shown in black. For termolecular reactions, complex rate constants are used and in these cases the low pressure limit (k_0), high pressure limit (k_1) and F_C value are specified.

CRI_v2_2_o1d

O(1D) + H2O = OH + OH : $k = 2.14 \times 10^{-10}$ cm^3 molecules^{-1} s^{-1}
O(1D) + H2O = OH + OH : $k = 2.20 \times 10^{-10}$cm^3 molecules^{-1} s^{-1}

O(1D) + N2 = OH + OH : $k = 2.00 \times 10^{-11} e^{130/T}$ cm^3 molecules^{-1} s^{-1}
O(1D) + N2 = OH + OH : $k = 1.80 \times 10^{-10} e^{110/T}$ cm^3 molecules^{-1} s^{-1}

O(1D) + O2 = OH + OH : $k = 3.20 \times 10^{-11} e^{67/T}$ cm^3 molecules^{-1} s^{-1}
O(1D) + O2 = OH + OH : $k = 3.20 \times 10^{-11} e^{70/T}$ cm^3 molecules^{-1} s^{-1}

CRI_v2_2_inorgN

O(3P) + NO = NO2: $k_0 = 1 \times 10^{-31}[M](T/300)^{-1.6}$, $k_1 = 5 \times 10^{-11}(T/300)^{-0.3}$ $F_C = 0.85$
O(3P) + NO = NO2: $k_0 = 9 \times 10^{-32}[M](T/300)^{-1.5}$, $k_1 = 3 \times 10^{-11}$ $F_C = 0.6$

O(3P) + NO2 = NO3: $k_0 = 1.30 \times 10^{-31}[M](T/300)^{-1.5}$, $k_1 = 2.30 \times 10^{-11}(T/300)^{0.24}$ $F_C = 0.6$
O(3P) + NO2 = NO3: $k_0 = 9 \times 10^{-32}[M](T/300)^{-2}$, $k_1 = 2.2 \times 10^{-11}$ $F_C = 0.6$

HO2 + NO2 = HO2NO2: $k_0 = 1.40 \times 10^{-31}[M](T/300)^{-3.1}$, $k_1 = 4.00 \times 10^{-12}$ $F_C = 0.4$
HO2 + NO2 = HO2NO2: $k_0 = 1.80 \times 10^{-31}[M](T/300)^{-3.2}$, $k_1 = 4.70 \times 10^{-12}$ $F_C = 0.6$

OH + NO = HONO: $k_0 = 7.40 \times 10^{-31}[M](T/300)^{-2.4}$, $k_1 = 3.30 \times 10^{-11}(T/300)^{-0.3}$ $F_C = 0.81$
OH + NO = HONO: $k_0 = 7.40 \times 10^{-31}[M](T/300)^{-2.4}$, $k_1 = 3.30 \times 10^{-11}(T/300)^{-0.3}$ $F_C = e^{-T/1420}$

OH + NO2 = HONO2: $k_0 = 3.20 \times 10^{-30}[M](T/300)^{-4.5}$, $k_1 = 3.00 \times 10^{-11}$ $F_C = 0.41$
OH + NO2 = HONO2: $k_0 = 2.60 \times 10^{-30}[M](T/300)^{-3.2}$, $k_1 = 2.40 \times 10^{-11}(T/300)^{-1.3}$ $F_C = 0.6$

MeCO3 + NO2 = PAN: $k_0 = 3.28 \times 10^{-28}[M](T/300)^{-6.87}$, $k_1 = 1.125 \times 10^{-11}(T/300)^{-1.105}$ $F_C = 0.30$
MeCO3 + NO2 = PAN: $k_0 = 8.50 \times 10^{-29}[M](T/300)^{-6.50}$, $k_1 = 1.10 \times 10^{-11}(T/300)^{-1.0}$ $F_C = 0.60$

EtCO3 + NO2 = PPAN: $k_0 = 3.28 \times 10^{-28}[M](T/300)^{-6.87}$, $k_1 = 1.125 \times 10^{-11}(T/300)^{-1.105}$ $F_C = 0.30$
EtCO3 + NO2 = PPAN: $k_0 = 8.50 \times 10^{-29}[M](T/300)^{-6.50}$, $k_1 = 1.10 \times 10^{-11}(T/300)^{-1.0}$ $F_C = 0.60$

NO2 + NO3 = N2O5 : $k_0 = 3.60 \times 10^{-30}[M](T/300)^{-4.10}$, $k_1 = 1.90 \times 10^{-12}(T/300)^{-0.2}$ $F_C = 0.35$
NO2 + NO3 = N2O5: $k_0 = 2.20 \times 10^{-30}[M](T/300)^{-3.90}$, $k_1 = 1.50 \times 10^{-12}(T/300)^{-0.7}$ $F_C = 0.60$

HOCH2CO3 + NO2 = PHAN : $k_0 = 3.28 \times 10^{-28}[M](T/300)^{-6.87}$, $k_1 = 1.125 \times 10^{-11}(T/300)^{-1.105}$ $F_C = 0.30$
HOCH2CO3 + NO2 = PHAN : $k_0 = 8.50 \times 10^{-29}[M](T/300)^{-6.50}$, $k_1 = 1.10 \times 10^{-11}(T/300)^{-1.0}$ $F_C = 0.60$

RTN26O2 + NO2 = RTN26PAN : $k_0 = 2.368 \times 10^{-28}[M](T/300)^{-6.50}$, $k_1 = 8.123 \times 10^{-11}(T/300)^{-1.105}$ $F_C = 0.30$
RTN26O2 + NO2 = RTN26PAN : $k_0 = 6.14 \times 10^{-29}[M](T/300)^{-6.87}$, $k_1 = 7.94 \times 10^{-12}(T/300)^{-1.0}$ $F_C = 0.60$

Note that RU12PAN, which exists in CS but not in CS2, was not added back into the mechanism for this test. In addition, the formation of MPAN, which involves RU10O2+NO2 in CS but MACO3+NO2 in CS2, was kept as MACO3+NO2 but the CS value of KFPAN was used. These changes are unlikely to have a significant impact since PAN dominated the total concentration of all PAN-type species.

MACO3 + NO2 = MPAN : $k_0 = 3.28 \times 10^{-28}[M](T/300)^{-6.87}$, $k_1 = 1.125 \times 10^{-11}(T/300)^{-1.105}$ $F_C = 0.30$
MACO3 + NO2 = MPAN : $k_0 = 8.50 \times 10^{-29}[M](T/300)^{-6.50}$, $k_1 = 1.10 \times 10^{-11}(T/300)^{-1.0}$ $F_C = 0.60$

HO2 + NO = OH + NO2 : $k = 3.45 \times 10^{-12}\, e^{270/T}$

HO2 + NO = OH + NO2 : $k = 3.60 \times 10^{-12}\, e^{270/T}$

OH + HO2NO2 = H2O + NO2 + O2 : $k = 3.20 \times 10^{-13}\, e^{690/T}$

OH + HO2NO2 = H2O + NO2 + O2 : $k = 1.90 \times 10^{-12}\, e^{270/T}$

OH + PAN = HCHO + CO + NO2 : $k = 3.40 \times 10^{-14}$

OH + PAN = HCHO + CO + NO2 : $k = 9.50 \times 10^{-13} e^{-650/T}$

OH + MPAN = CARB7 + CO + NO2 : $k = 6.38 \times 10^{-12}$

OH + MPAN = CARB7 + CO + NO2 : $k = 3.60 \times 10^{-12}$

OH + MeONO2 = HCHO + NO2 + H2O: $k = 4.00 \times 10^{-13} e^{-845/T}$

OH + MeONO2 = HCHO + NO2 + H2O: $k = 1.00 \times 10^{-14} e^{-1060/T}$

MeOO + NO = HCHO + NO2 + HO2: $k = 2.298 \times 10^{-12} e^{-360/T}$

MeOO + NO = HCHO + NO2 + HO2: $k = 3.00 \times 10^{-12} e^{-280/T}$

MeOO + NO = MeONO2 : $k = 2.30 \times 10^{-15} e^{-360/T}$

MeOO + NO = MeONO2 : $k = 3.00 \times 10^{-15} e^{-280/T}$

MeOO + NO3 = HO2 + HCHO + NO2 : $k = 1.20 \times 10^{-12}$

MeOO + NO = HO2 + HCHO + NO2 : $k = 1.00 \times 10^{-12}$

CRI_v2_2_isoprene

In this branch, changes were made to the isoprene oxidation scheme to bring it as close as was practicable to that used in CRI-STRAT. The major changes were the removal of the isomerisation reactions of the isoprene peroxy radical, RU14O2, and the updated oxidation pathway of the species UCARB10 which represents the major isoprene oxidation products methacrolein (MACR) and methyl vinyl ketone (MVK).

In this branch RU14O2 only underwent reactions with HO2, NO, NO3 and RO2. This meant the production of 10 of the 12 new CRI v2.2 species (IEPOX, HMML, HPUCARB12, HUCARB9, DHPR12OOH, DHPCARB9, DHCARB9, MACO3, DHPR12O2 and RU10AO2) and their subsequent reactions, which are key in the HOx-recycling process, were removed from the mechanism. Note that the production of two new organonitrate species, RU12NO3 and RU10NO3, and their subsequent reaction were maintained as these had much less to do with the HOx-recycling feature under examination. It should also be noted that where there was a difference between the rate constants in CS and CS2 for a given reaction (e.g. changes in the RO2+NO and RO2+NO3 rate constants), the rate constant from CRI v2.2 was used to minimise the other drivers for difference that was observed between this branch and the full CRI v2.2 branch.

In addition, all isoprene oxidation reactions with OH, O3 and NO3 were reverted to those in CS.

NO3 + C5H8 = NRU14O2 : $k = 3.15 \times 10^{-12} e^{-450/T}$

NO3 + C5H8 = NRU14O2 : $k = 3.0 \times 10^{-12} e^{-466/T}$

O3 + C5H8 = UCARB10 + CO + HO2 + OH : $k = 1.288 \times 10^{-15} e^{-1995/T}$

O3 + C5H8 = HCHO + MeOO + CO + HO2 : $k = 9.79 \times 10^{-16} e^{-1995/T}$

O3 + C5H8 = UCARB10 + HCOOH : $k = 1.80 \times 10^{-15} e^{-1995/T}$

O3 + C5H8 = UCARB10 + HCHO + H2O2 : $k = 3.97 \times 10^{-15} e^{-1995/T}$
O3 + C5H8 = MeCO3 + HCHO + CO + OH : $k = 1.29 \times 10^{-15} e^{-1995/T}$
O3 + C5H8 = UCARB10 + CO : $k = 9.785 \times 10^{-16} e^{-1995/T}$
O3 + C5H8 = UCARB10 + CO + HO2 + OH : $k = 2.12 \times 10^{-15} e^{-1913/T}$
O3 + C5H8 = UCARB10 + HCOOH : $k = 5.74 \times 10^{-15} e^{-1913/T}$

OH + C5H8 = RU14O2 : $k = 2.70 \times 10^{-12} e^{390/T}$
OH + C5H8 = RU14O2 : $k = 2.54 \times 10^{-12} e^{410/T}$

OH + UCARB10 = RU10O2 : $k = 3.84 \times 10^{-12} e^{533/T}$
OH + UCARB10 = RU10O2 : $k = 2.50 \times 10^{-11}$

NO3 + UCARB10 = RU10O2 + HONO2: $k = 5.98 \times 10^{-13} e^{-1862/T}$
NO3 + UCARB10 = RU10O2 + HONO2 : $k = 1.44 \times 10^{-12} e^{-1862/T}$

O3 + UCARB10 = HCHO + MeCO3 + CO + OH : $k = 3.84 \times 10^{-16} e^{-1710/T}$
O3 + UCARB10 = HCHO + MeCO3 + CO + OH : $k = 1.68 \times 10^{-18}$

O3 + UCARB10 = HCHO + CARB6 : $k = 8.16 \times 10^{-16} e^{-1710/T}$
O3 + UCARB10 = HCHO + CARB6 + H2O2 : $k = 1.17 \times 10^{-18}$

OH + UCARB12 = RU10O2 : $k = 6.42 \times 10^{-11}$
OH + UCARB12 = RU10O2 : $k = 4.52 \times 10^{-11}$

NO3 + UCARB12 = RU10O2 : $k = 6.42 \times 10^{-11}$
NO3 + UCARB12 = RU10O2 : $k = 4.52 \times 10^{-11}$

O3 + UCARB12 = HOCH2CHO + MeCO3 + CARB3 + OH : $k = 6.00 \times 10^{-18}$
O3 + UCARB12 = HOCH2CHO + MeCO3 + CO + OH : $k = 2.14 \times 10^{-17}$

O3 + UCARB12 = CARB6 + CO + OH + HO2 : $k = 1.20 \times 10^{-17}$
O3 + UCARB12 = HOCH2CHO + CARB6 + H2O2 : $k = 2.64 \times 10^{-18}$

UCARB12 = MeCO3 + HOCH2CHO + CO + HO2:$0.25 * jmacr$
UCARB12 = MeCO3 + HOCH2CHO + CO + HO2: $jmacr$

UCARB12 = RU12O2 + HO2:$0.5 * jmacr$
No replacement

UCARB12 = RU12O2 + CARB7 + CO :$0.25 * jmacr$
No replacement

NRU12OOH = NOA + CARB3 + HO2 + OH: $jhmp$
NRU12OOH = NOA + CO + HO2 + OH : $jhmp$

NUCARB12 = HUCARB9 + CO + NO2 + OH: $jmacr$
NUCARB12 = NOA + 2*CO + 2*HO2 : $jmacr$

NUCARB12 = CARB7 + CO + HO2 + NO2:$8 * jnoa$
No replacement

All reactions of HUCARB9, HPUCARB12, DHCARB9, DHPCARB9, RU10AO2, MACO3, DHPR12O2, DHPR12OOH and IEPOX and HMML were removed. Reactions which produced these species reverted to their CS equivalents.

OH + RU14OOH = 0.09UCARB12 + 0.94OH + 0.85IEPOX + 0.06RU14O2: $k = 7.14 \times 10^{-11}$
OH + RU14OOH = UCARB12 + OH: $k = 7.51 \times 10^{-11}$

OH + RU12OOH = RU10OOH + CO + HO2: $k = 3.50 \times 10^{-11}$

OH + RU12OOH = RU12O2: $k = 3.00 \times 10^{-11}$

OH + RU10OOH = CARB7 + CO + OH: $k = 3.84 \times 10^{-11}$
OH + RU10OOH = RU10O2: $k = 3.00 \times 10^{-11}$

MPAN + OH = HMML + NO3: $k = 2.262 \times 10^{-11}$
No replacement

MPAN = MACO3 + NO2: $k = 1.60 \times 10^{16} e^{-13500/T}$
MPAN = RU10O2 + NO2: $k_0 = 1.10 \times 10^{-5} e^{-10100/T}$, $k_1 = 1.90 \times 10^{17} e^{-14100/T}$ $F_C = 0.30$

MACO3 + NO2 = MPAN : $k_0 = 3.28 \times 10^{-28}[M](T/300)^{-6.87}$, $k_1 = 1.125 \times 10^{-11}(T/300)^{-1.105}$ $F_C = 0.30$
MACO3 + NO2 = MPAN : $k_0 = 8.50 \times 10^{-29}[M](T/300)^{-6.50}$, $k_1 = 1.10 \times 10^{-11}(T/300)^{-1.0}$ $F_C = 0.60$

RU14O2 = UCARB10 + HCHO + OH
No replacement

RU14O2 = 0.5 HPUCARB12 + 0.5 HO2 + 0.5 DHPR12O2
No replacement

RU10AO2 + NO3 = CARB7 + HCHO + HO2 + NO2 : $k = 2.30 \times 10^{-12}$
RU10O2 + NO3 = CARB7 + HCHO + HO2 + NO2 : $k = 5.00 \times 10^{-13}$

RU10AO2 + RO2 = CARB7 + CO + HO2 : $k = 3.60 \times 10^{-13}$
RU10O2 + RO2 = CARB7 + HCHO + HO2 : $k = 4.00 \times 10^{-13}$

RU12O2/RU10O2 - aside from changes from RU10AO2 to RU10O2, no other changes made

CRI_v2_2_RO2_N

The only change made to the mechanism for this test was reversion of the rate constants of RO2 with NO and NO3. Where branching ratios had changed between CS and CS2, the CRI v2.2 were maintained with rate constants scaled accordingly. The red rate constants below were changed to those in black:

kRO2NO: $k = 2.70 \times 10^{-12} e^{360/T}$
kRO2NO: $k = 2.40 \times 10^{-12} e^{360/T}$

kRO2NO3: $k = 2.30 \times 10^{-12}$
kRO2NO:3 $k = 2.50 \times 10^{-12}$

Five acyl peroxy species in CRI featured a different RO2 + NO rate constant, kAPNO, which decreased by 7.5% in CRI v2.2.

kAPNO: $k = 7.50 \times 10^{-12} e^{290/T}$
kAPNO:3 $k = 8.10 \times 10^{-12} e^{290/T}$

Section S3 iBVOC and Megan-MACC Emissions

The difference between two possible BVOC emissions approaches, the iBVOC approach and the non-interactive MEGAN-MACC emission approach, was considered. Globally, the annual average non-interactive isoprene emissions were 5.9% higher (576.9 Tg yr^{-1} vs. 545.0 Tg yr^{-1}) while MT emissions

were 29% lower (97.5 Tg yr^{-1} v. 137.3 Tg yr^{-1}, cf 95±3 Tg yr^{-1} Sindelarova et al., 2014) (Fig. S1). Emissions at three of the surface observational sites, ATTO, Z2F and Borneo, were also compared with a specific focus on the months where model-observational comparisons were performed. At the ATTO and Z2F sites monthly MEGAN-MACC isoprene emissions were lower than iBVOC emissions (~ 40% for the months considered). Non-interactive MT emissions at the ATTO sites were also lower than iBVOC emissions (35% Feb and 25% Sept) but slightly higher in June for the Z2F site. In Borneo, MEGAN-MACC isoprene and MT emissions were ~25% and ~15% lower than iBVOC over the April-July period respectively.

A spatial comparison of the emission approaches was also performed (Fig. S2). Annually averaged, iBVOC exhibited greater isoprene emissions in the northern part of South America but lower emissions at more southern latitudes as well as general southern migration of isoprene emissions in Africa. Isoprene emissions in Australia were significantly lower. These differences were more pronounced in the June-July-August (JJA) period while in the December-January-February (DJF) period iBVOC also exhibited increased emissions over China and South East Asia and the northern hemisphere boreal forests but lower emissions over the South East USA. For monoterpenes, iBVOC simulated greater JJA emissions in the boreal forest, South East USA and South East Asia and greater DJF emissions in much of South America.

Figure S1. Global emissions of (a) isoprene and (b) MT from the non-interactive MEGAN-MACC (MM) dataset and iBVOC (shading shows standard deviations in iBVOC emissions over period

2005-2013). Emissions per unit area for isoprene and MT at the ATTO (c, d), Bannan (e, f) and Borneo (g, h) observational sites. Black dots indicate months when model-observational comparisons were performed at the corresponding site.

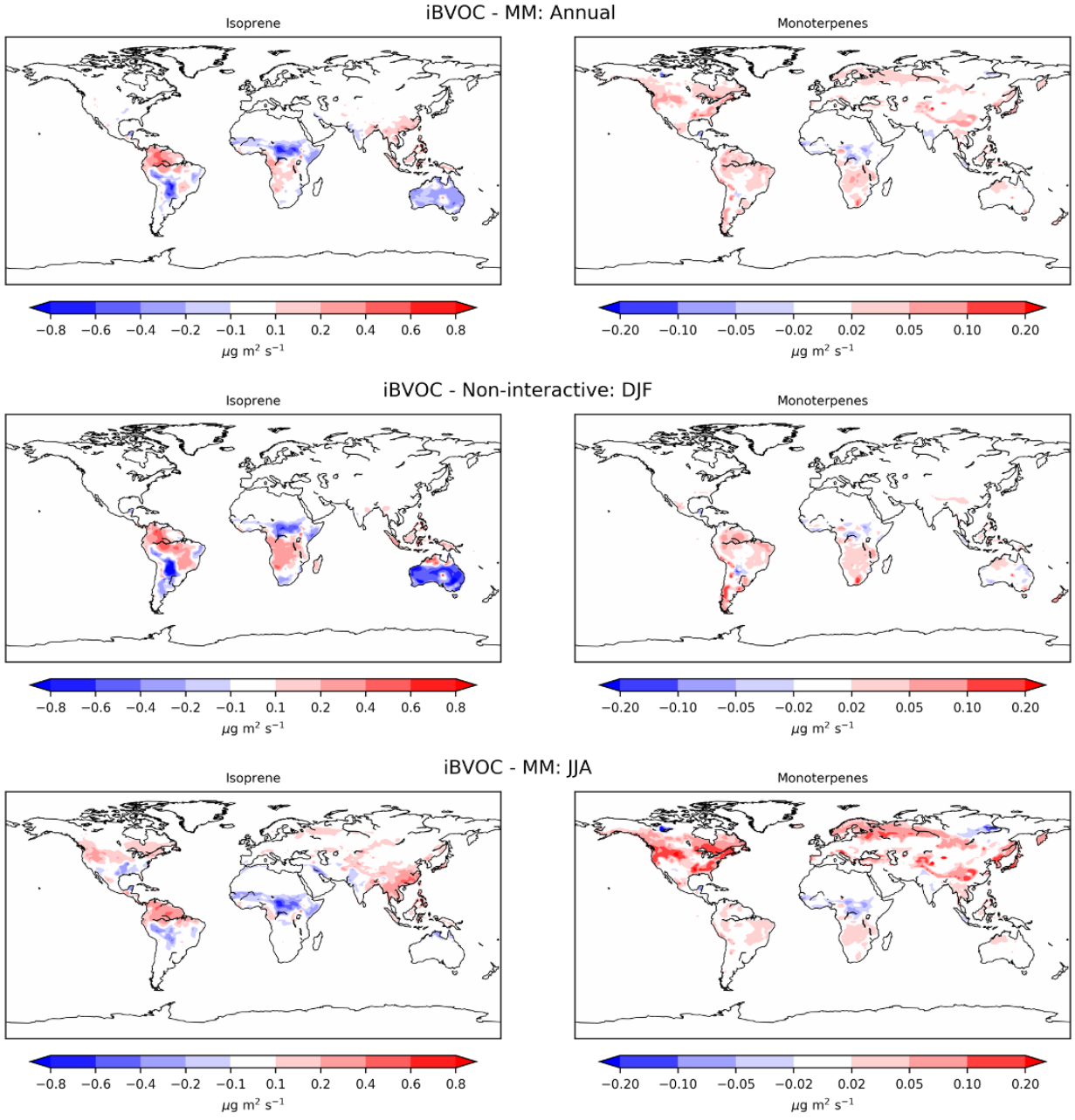

Figure S2. Difference in emissions between the iBVOC and MEGAN-MACC 2001-2010 climatologies (MM) emission approaches for isoprene and monoterpenes. Annual average (top panels), DJF average (middle panels) and JJA average (lower panels).

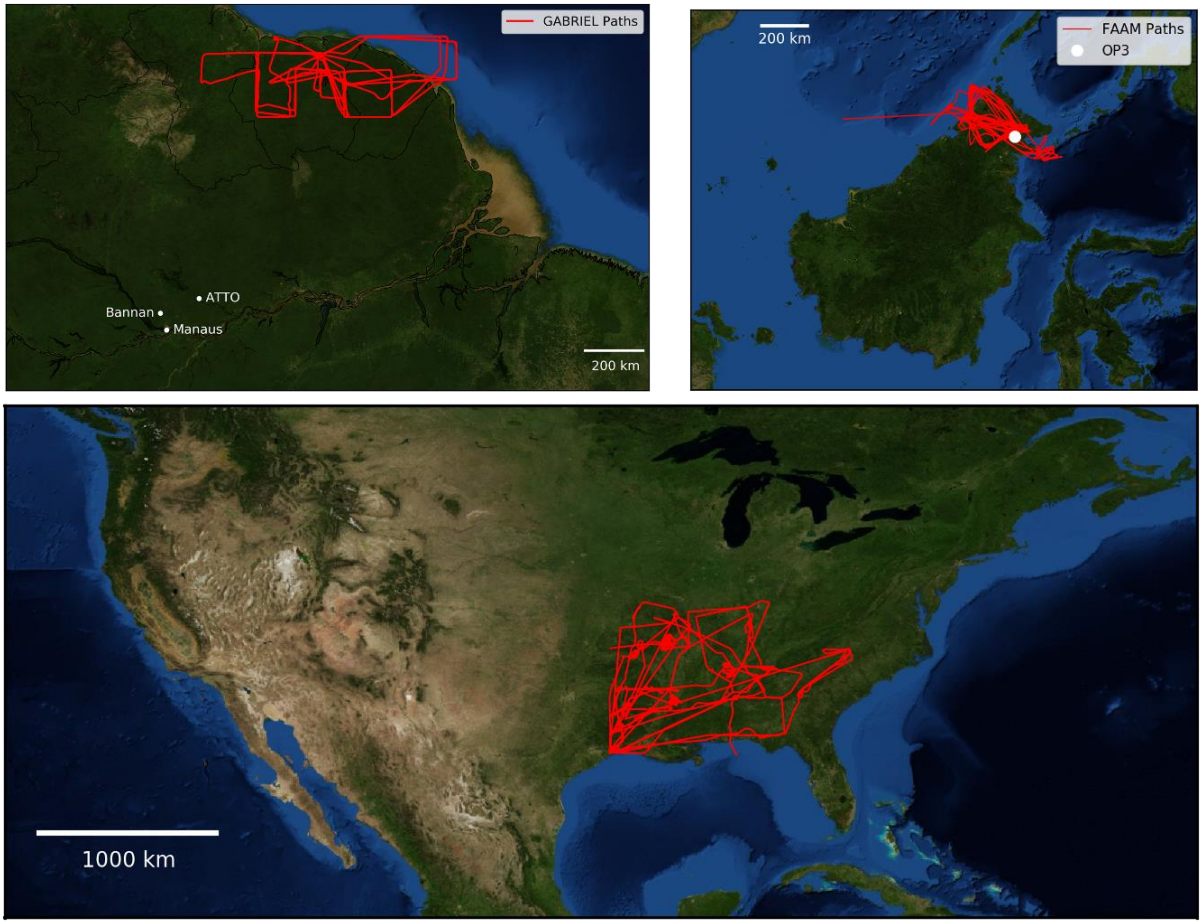

Figure S3. Location of the two in-situ Amazon observation sites (Bannan and ATTO), city of Manuas and GABRIEL aircraft campaign paths (upper left), OP3 observation tower and FAAM aircraft campaign flights over Borneo (upper right) and SEAC^{4}RS flight campaign over the South East USA (lower). Map Sources: Esri, DigitalGlobe, GeoEye, i-cubed, USDA FSA, USGS, AEX, Getmapping, Aerogrid, IGN, IGP, swisstopo, and the GIS User Community

Table S3 – Additional information regarding observational data

Dataset	Notes
SEAC^{4}RS	All data points below limit of detection set to zero
GABRIEL	Estimated LODs: Isoprene 0.1 ppb, MVK 0.09 ppb, Acetone 0.09 ppb Non-zero data points below the LOD were not removed.
FAAM	Estimated LOD: Isoprene 0.1 ppb Data marked as low quality was ignored
Borneo	Data marked as low quality was ignored
ATTO	Monoterpene LOD: 0.05 ppb (Sept 2013) 0.06 ppb (March 2014) Isoprene LOD: 0.09 ppb (Feb 2013), 0.1 ppb (Sept 2013) Acetone LOD: 0.03 ppb (Feb 2013), 0.05 ppb (Sept 2013) Isoprene oxidation products LOD: 0.13 ppb (Feb 2013), 0.07 ppb (Sept 2013)

	LOD estimated as 2σ of the background average. Non-zero data points below the LOD were not removed.

Section S4 Overview of field Brazil ZF2 measurements

A suite of online measurement techniques was deployed in Central Amazonia, at the ZF2 site located 61 km north upwind of Manaus (60°11'W, 2°5'S) in June and July 2016. This is a site that at the transition between wet and dry seasons that is mostly influenced by natural biogenic emissions, with virtually no biomass burning and no anthropogenic pollution at the time of experiment. A high-resolution TOF-CIMS using iodide-adduct ionization was coupled to an Aerodyne Research Incorporated FIGAERO (Lee et al., 2014, Lopez-Hilfiker et al., 2015, Bannan et al., 2019), and was utilized for the semi-simultaneous measurement of a range of oxygenated species in the gas and particle phase. An Aerodyne ACSM (Aerosol Chemical Speciation Monitor) monitored the bulk submicron organic and inorganic aerosol composition and a PTR-MS (proton transfer reaction mass spectrometer) was used to measure isoprene and a subset of isoprene oxidation products. Routine measurements including NO_x, SO_2 and O_3 and key meteorological conditions were also made. Further details of all aspects of the field measurements are given in the sections that follow.

TOF-CIMS technique

Configuration and operating technique

The gas-phase measurements of the Manchester time-of-flight chemical ionization mass spectrometer (TOF-CIMS) instrument have been described in detail previously (Priestley *et al*, 2015) but the specific setup and operation procedures used in the present work is described herein. The instrument comprises an Aerodyne FIGAERO inlet attached to a reduced pressure ion molecule reaction (IMR) region in front of a Tofwerk atmospheric pressure interface high resolution time-of-flight mass spectrometer (Lopez-Hilfiker et al., 2015) together these facilitate simultaneous gas and particle phase measurements. In the present work, a Tofwerk X-Ray ionization source was used in place of the Po-210 source normally used with iodine CIMS. The instrument performance was tracked daily by monitoring the baseline, single ion signal measurements, m/z calibrations, regular gas-phase calibrations and high-frequency filter and gas-phase background measurements.

The Aerodyne FIGAERO is a two-port inlet with the first dedicated to gas sampling (PFA Teflon tubing, 20 SLM measured flow rate) and the second to aerosol sampling (stainless steel inlet,10 SLM measured flow rate). The sampling lines were situated at an altitude just above the canopy to avoid sampling being compromised by trees or structures. Recently, Liu *et al. (2016)* discussed in detail the effect of inlets on species quantification - the inlets used in the present work were chosen due to the limitations of the measurement site.

The FIGAERO couples both inlets with the chemical ionization region of the mass spectrometer and operates in two modes: (A) ambient air sampling for trace gas analysis using CIMS and simultaneous particle collection on a PFTE filter via a separate inlet, and, (B) thermal desorption of the collected particles in nitrogen, allowing detection of the desorbed vapors via CIMS.

The IMR was held at a constant pressure by a scroll pump (Agilent SH-112), regulated with a servo control valve placed between the scroll pump and IMR. The ionizing reagent, I-, was generated via X-ray ionization of CH_3I. 10 sccm of N_2 was flowed over a methyl iodide (CH_3I) permeation tube (held at 40°C) and the resultant CH_3I-entrained N_2 carried by a 2 SLM N_2 flow through the X-ray ionizer into the IMR, orthogonally to the sample flow. The ionizer and ambient air flows were allowed to mix, such that trace chemical species within the ambient air sample were ionized by I-, generating iodine adducts. The resultant flow was sampled via a critical orifice into the first of four differentially pumped chambers in the TOF-CIMS. The first chamber was held at a set pressure (1.6 mbar) by a scroll pump (Triscroll 600)

and the subsequent chambers were pumped by a split flow turbo molecular drag pump. Quadrupole ion guides transmitted the ions through these chambers while simultaneously providing additional collisional cooling and energetic homogenization of the ions as they entered the extractor region. The electric fields were set to optimize the total ion signal and transmission of the iodide adducts.

CIMS Calibrations and background measurements

Mass calibration was performed using 5 known masses (I^-, $I^-.H_2O$, $I^-.HCOOH$, I_2^- and I_3^-) that cover a range of m/z 127 to 380. The mass calibration was fitted by a 3rd order polynomial and was accurate to within 1 ppm, ensuring peak identification for all species was accurate below 1 ppm. The Tofware-specific FIGAERO-CIMS analysis software (version 3.1) was utilized to attain high-resolution 1Hz time series of all of the species identified here, in both the gas- and particle-phases. Further analysis was done using software developed in-house.

Gas-phase background measurements were made once every 30 minutes for 30 seconds by overflowing the IMR just above the pinhole with wetted high-purity nitrogen. Data was background-subtracted using an interpolation of the two background measurements recorded either-side of data collection. An example of the data processing for an arbitrary mass is shown in Figure S1.

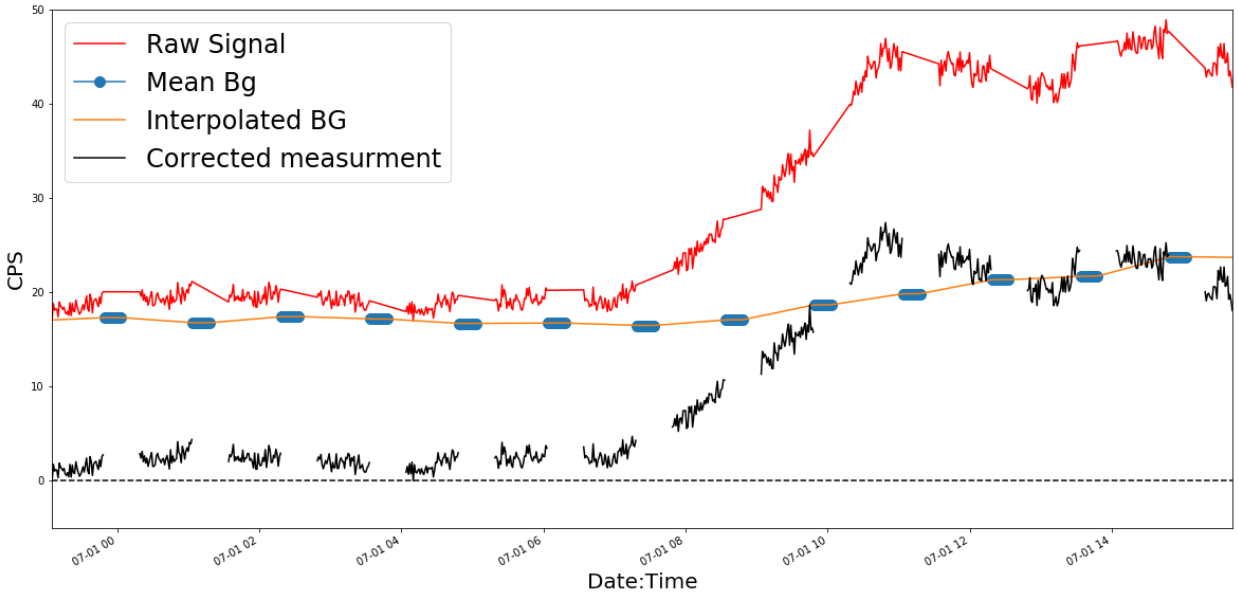

Fig. S4 Retrieval of background-corrected data from raw data for a subset of the measurement campaign for an arbitrary mass. The background counts obtained during the background period (blue dots) are interpolated to yield the interpolated background data (orange line). This is subtracted from the raw signal (red line) to obtain the corrected measurement (black line). All data are in units of counts per second (CPS).

Background filter measurements comprised a ramp, soak and cool cycle matching that of the ambient air sampling method. Each background measurement was applied to the thermogram measurements made until the next background filter measurement was recorded. In the event of a break in FIGAERO-CIMS measurements (i.e., due to temporary failure or power shortages), a new filter was placed into the instrument. The new filter was cleaned by ramping the temperature to 200°C for a duration of 20 mins and subsequently cooled, with a complete cycle immediately after. Where there was no break in the

measurements for ~2 days, the cleaning process was undertaken for the existing installed filter. Detailed analysis during the measurements was undertaken to ensure that all of the collected material was being volatilized during normal operation.

Offline calibrations after the field work campaign were performed specific to the isoprene oxidation species that were observed at the ZF2 site. 2-Methyltetrols, 2-methylglyceric acid, and IEPOX were synthesized by the University of North Carolina, Department of Environmental Sciences & Engineering according to procedures outline in Bondy et al. (2018), Budisulistiorini et al. (2015), and Zhang et al. (2012), respectively. These standards were dissolved in acetone at known concentrations and using a micro-syringe were deposited on the FIGAERO filter and thermally desorbed using a known continuous flow of nitrogen over the filter. This was performed following the methodology devised in Lee et al. (2014). The measured sensitivities for $C_5H_{10}O_3$, $C_4H_8O_4$, $C_5H_{12}O_4$ varied by a maximum of 25% from each other with the mean sensitivity of the 3 isoprene oxidation standards being only 8% higher than that of acetic acid. The mean sensitivity of the 3 isoprene oxidation standards in the gas and particle phase is therefore applied to the full data set presented here.
All species sensitivities reported herein were deduced assuming a linear response between reported and formic acid calibrations in the field (where day-to-day calibrations were performed) and the laboratory. A range of other species were calibrated for after the campaign, and relative calibration factors were derived using the measured formic acid sensitivity during these calibrations, as has been performed previously (Le Breton *et al.*, 2018; Bannan et al., 2015)

Supporting measurements

Several supporting measurements were made that allow for interpretation of the TOF-CIMS measurements. These include gas-phase measurements of biogenic volatile organic compounds (BVOCs) from a proton transfer time-of-flight mass spectrometer (PTR-ToF-MS; Ionicon Analytik) and particle-phase measurements using an aerosol chemical speciation monitor (ACSM)(DeCarlo *et al.*, 2006). Operation and analysis procedures are outlined elsewhere for the PTR-TOFMS (Liu *et al.*, 2016) and for the ACSM (de Sá *et al., 2017)*. The chemical composition of submicrometer aerosols was measured on-line by mass spectrometry using an Aerosol Chemical Speciation Monitor (ACSM). The aerosol mass spectrometer was used to characterize a wide range of non-refractory sub-micron aerosol particles such as organics, nitrate, sulfate, ammonium, and chloride in real-time with time-resolution of <15 minutes. Sulfur dioxide, NO_x and O_3 mixing ratios were monitored at both sites using trace gas analyzers (Thermo 43i-TLE, Thermo 42i and Thermo 49i, respectively). Meteorological parameters were measured using two different automatic weather stations (HOBO U30 Station GSM-UDP). Meteorological measurements comprised: temperature (± 0.3 °C), humidity (± 3–5%), rain amount (± 5% for daily accumulation), wind speed (0.3–0.5 ms-1) and direction (± 3°), where the resolution and accuracy are stated in parenthesis.

837

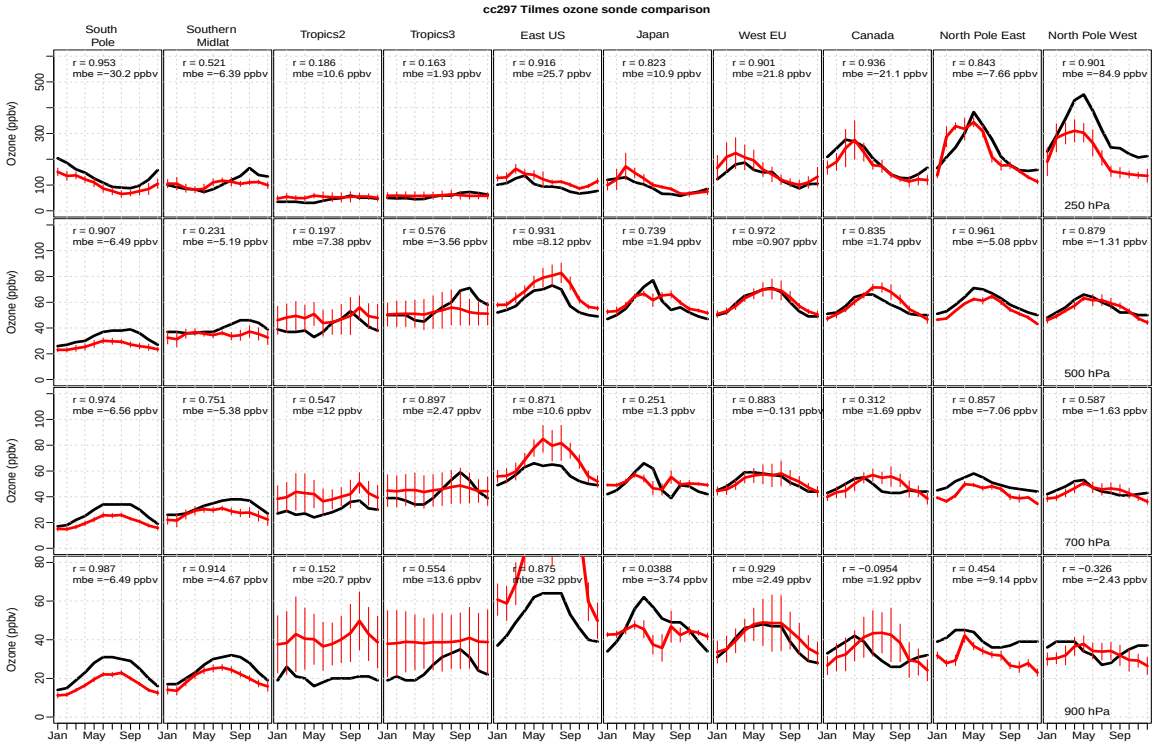
cc297 Tilmes ozone sonde comparison
South Pole
Southern Midlat
Tropics2
Tropics3
East US
Japan
West EU
Canada
North Pole East
North Pole West
Ozone (ppbv)
250 hPa
500 hPa
700 hPa
900 hPa
Jan
May
Sep

838

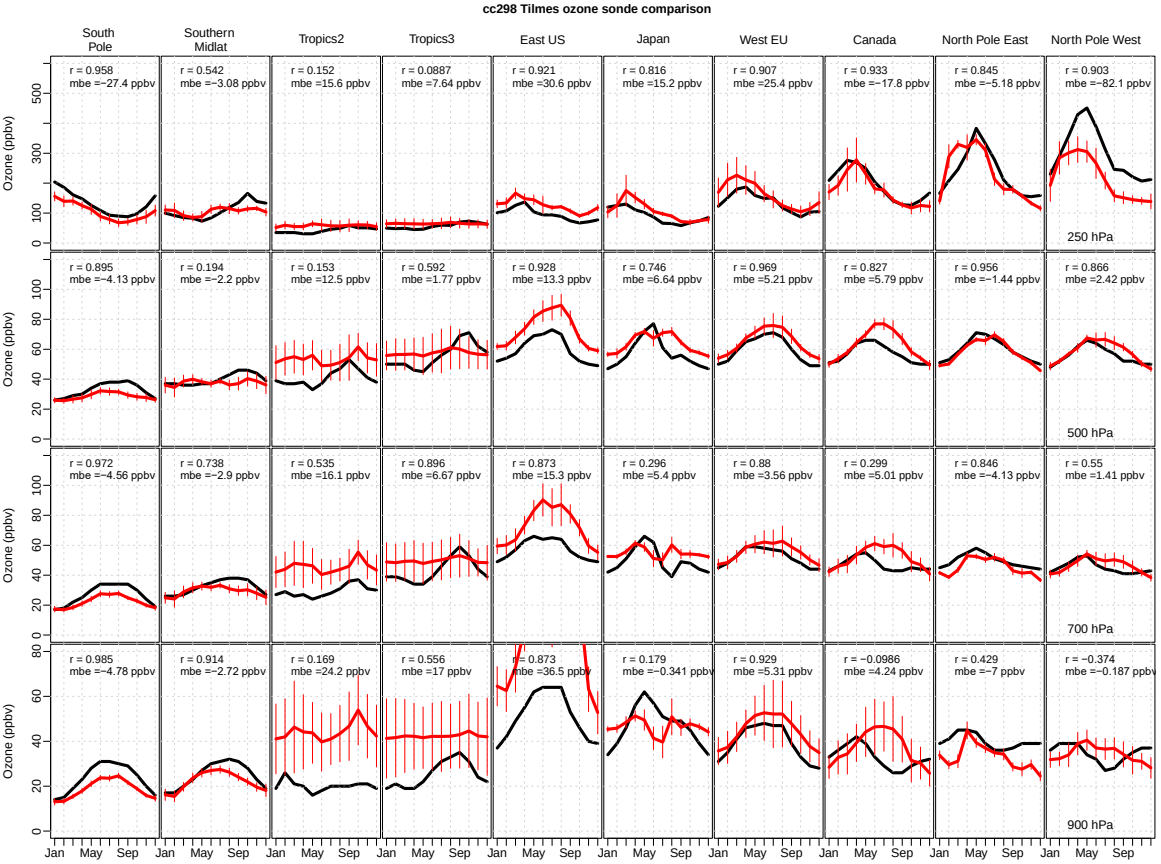
cc298 Tilmes ozone sonde comparison
South Pole
Southern Midlat
Tropics2
Tropics3
East US
Japan
West EU
Canada
North Pole East
North Pole West
Ozone (ppbv)
250 hPa
500 hPa
700 hPa
900 hPa
Jan
May
Sep

839

Figure S5 - Monthly mean ozone from observations (black) and CS (cc297 upper plot, red) and CS2 (cc298 lower plot, red) runs at 10 sites and 4 pressure levels (250 hPa – 1st row, 500 hPa – 2nd row, 700 hPa – 3rd row, 900 hPa – 4th row) .

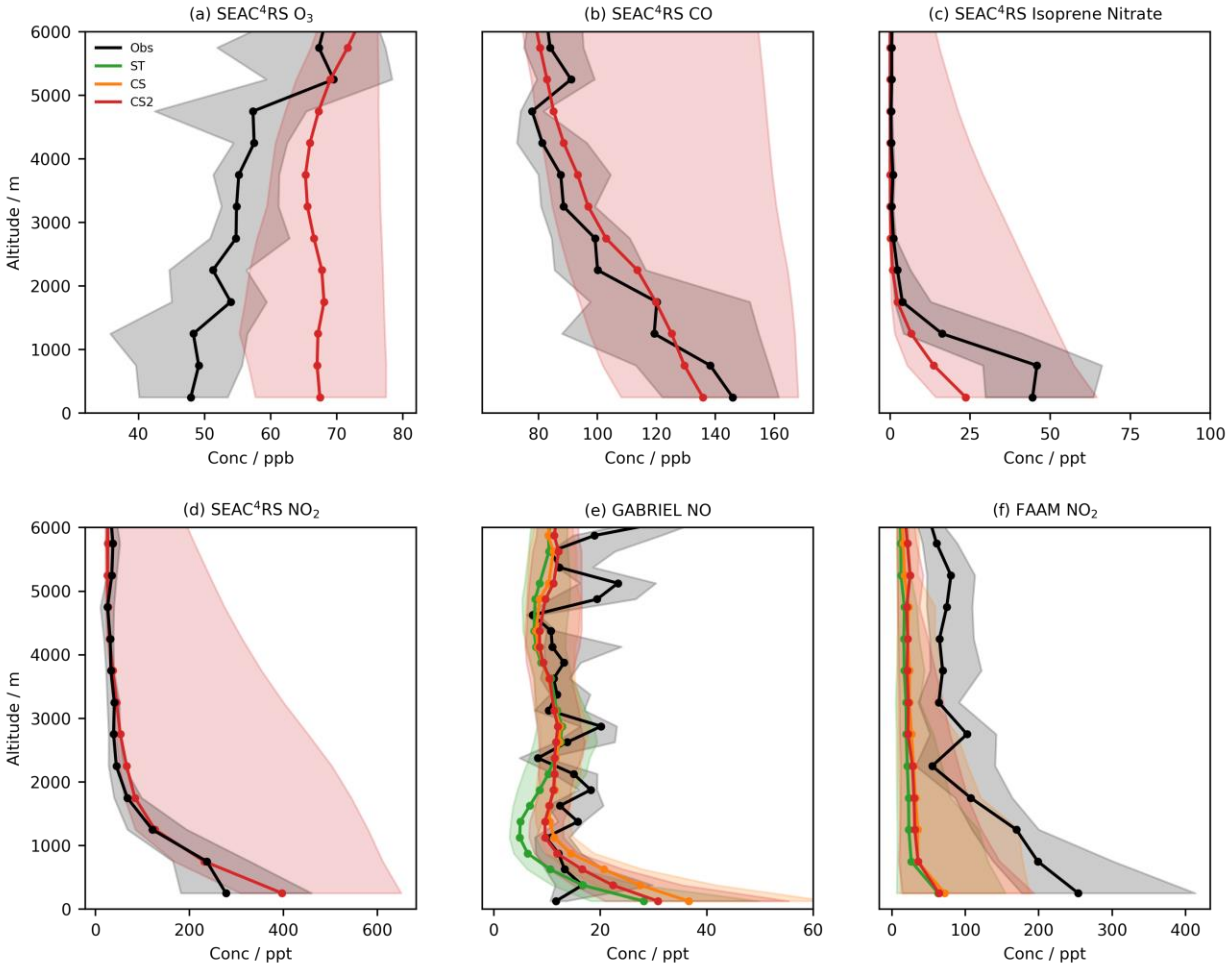

Figure S6 - Median observed and model (CS2) concentrations for (a) O_3, (b) CO, (c) Isoprene nitrate, (d) NO_2 from the SEAC^{4}RS flight campaign. Panels (e) and (f) show median observed NO (GABRIEL) and NO_2 (FAAM) concentrations from observations and all mechanisms. Shading shows IQR.

Section S5 Other Species

CO

As discussed in the context of HO_x, Borneo modelled surface CO was high biased for all mechanisms (Fig. S7) with CS and CS2 exhibiting a bias 50-60 ppb in July when observations were low (~100 ppb) and ST a bias of 27 ppb. ST and CS were low and high biased respectively by around 13 ppb while CS2 was high biased by 27 ppb (Fig. S10). Over the Amazon CS and CS2 exhibit a smaller low bias than ST

while over Borneo, ST and CS perform well with ST high biased by 10-15 ppb (Fig. 3). The CO profile from CS2 performs well against SEAC^{4}RS data (Fig. S5).

Monthly mean surface CO from the longer CS2 runs show a consistent increase across multiple locations in CO concentration compared to CS but, due to the spatially-varying performance of CS (high bias in certain regions and low bias in others), CS2 appeared no better or worse than CS on a global scale. A small increase in low altitude CO was also seen in the annual mean CO vertical profiles.

$HONO_2$

Tropospheric vertical profiles of annual mean nitric acid at multiple locations show a small increase in CS2 in a few locations (<~50 ppt) relative to CS, slightly increasing the general model high bias. In the stratosphere, $HONO_2$ was slightly (0.25-0.5 ppb) lower than CS in the 20-30 km increasing the model low bias.

Benzene and SO_2

In the Amazon CS and CS2 show reasonable agreement for benzene while all mechanisms have a daytime low bias for SO_2 (Fig. S10).

PAN

PAN is high biased in Borneo (Fig S7), with CS and CS2 worse than ST. The increase in PAN in CS is documented by Archer-Nicholls et al (2021) and the general reduction from CS to CS2 is discussed in Section 4.

HCHO

The model high bias for HCHO in Borneo (Fig. S7) increased from ST to the CS due to additional secondary production (Archer-Nicholls et al., 2021) while above the Amazon, CS2 (Fig. S10) did yield an improvement relative to CS at low altitudes (< 1km). The general reduction in HCHO in CS2 relative to CS is discussed further in Section 5.

Acetone and Acetaldehyde

All mechanisms are significantly high biased for acetone and acetaldehyde in Borneo and for acetone in the Amazon (Figs S7, S8). Above the Amazon, the three mechanisms are broadly similar for acetone displaying high bias at low altitude (greatest in the CRI mechanisms due to enhanced secondary production) and much smaller bias above ~ 2km. This highlights the importance of the ongoing work to update the photolysis of acetone and acetaldehyde species. These updates which are yet to be incorporated in UKCA have been noted to increase acetone photolysis frequency by 3-5x in the lowest 5km (Prather et al., 2013) and so should help to reduce model high bias.

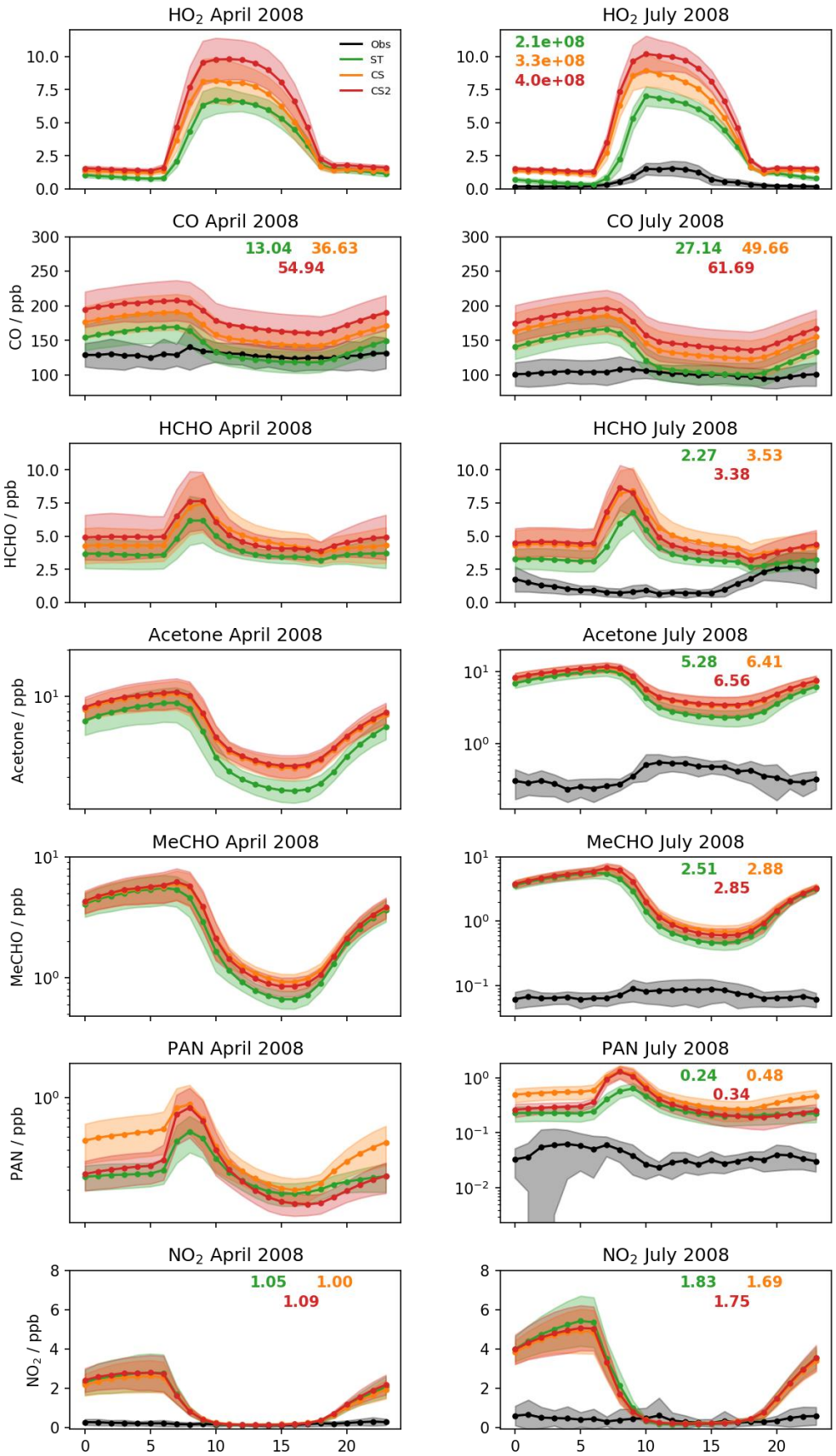
HO2 April 2008
HO2 July 2008
Obs
ST
CS
CS2
2.1e+08
3.3e+08
4.0e+08
CO April 2008
CO July 2008
CO / ppb
13.04 36.63
54.94
27.14 49.66
61.69
HCHO April 2008
HCHO July 2008
HCHO / ppb
2.27 3.53
3.38
Acetone April 2008
Acetone July 2008
Acetone / ppb
5.28 6.41
6.56
MeCHO April 2008
MeCHO July 2008
MeCHO / ppb
2.51 2.88
2.85
PAN April 2008
PAN July 2008
PAN / ppb
0.24 0.48
0.34
NO2 April 2008
NO2 July 2008
NO2 / ppb
1.05 1.00
1.09
1.83 1.69
1.75

Figure S7 - Mean modelled (ST, CS and CS2) and observed diurnal profiles of HO_2, CO, HCHO, Acetone, MeCHO, PAN and NO_2 profiles from Borneo. Observations are from the OP3 tower (ref) and model output from the most relevant grid cell. Shading indicates ±1 standard deviation from the mean and the numbers in bold show the mean diurnal model bias (model - observations) for species/locations where observations were recorded.

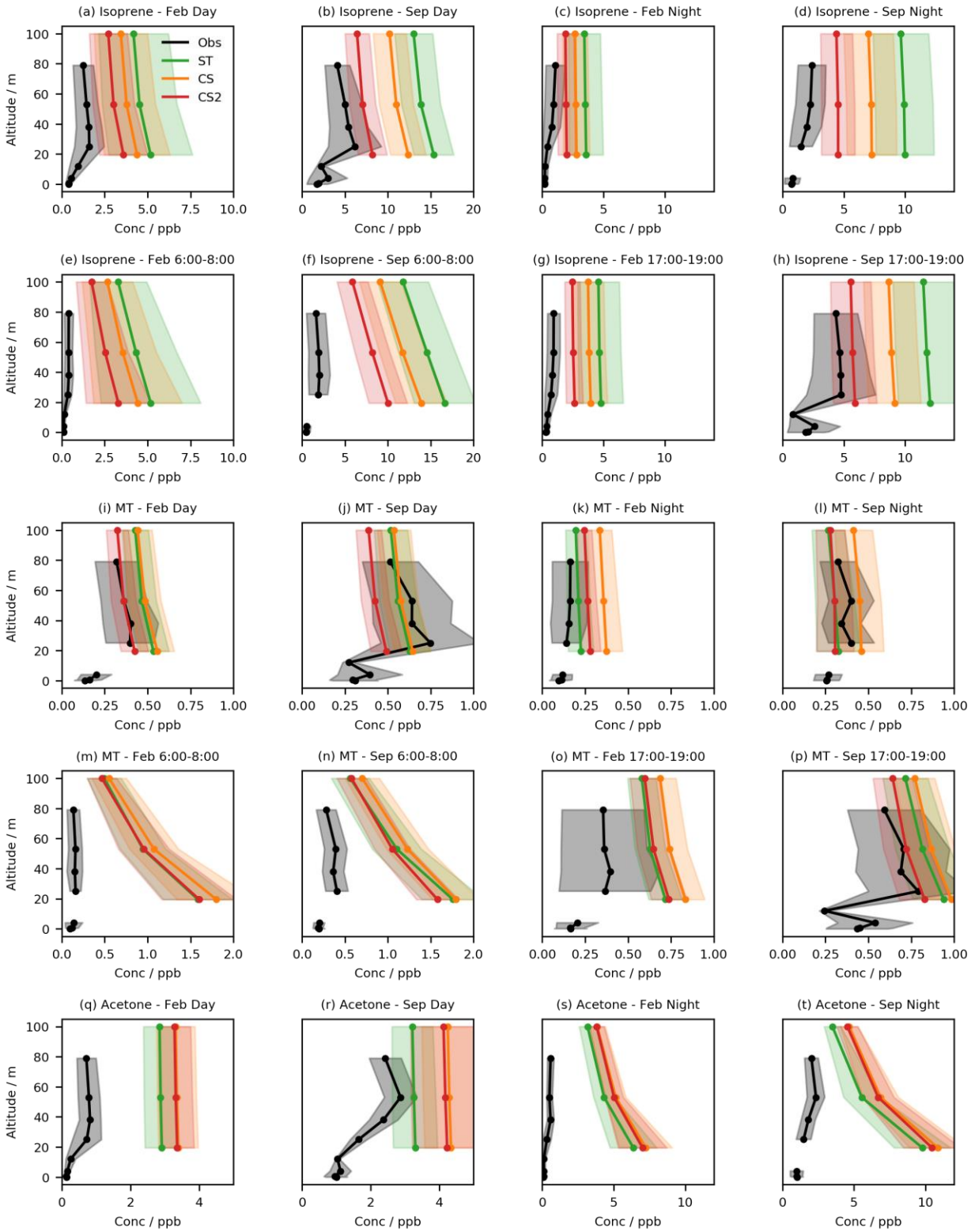

Figure S8 - Mean vertical profiles of isoprene, monoterpenes from observations taken at the ATTO tower (Yanez-Serrano et al., 2015) and model output from ST, CS and CS2. Daytime and nighttime

periods are taken as 9:00-15:00 and 21:00-03:00 respectively. Shaded regions indicate ± 1 standard deviation from the mean.

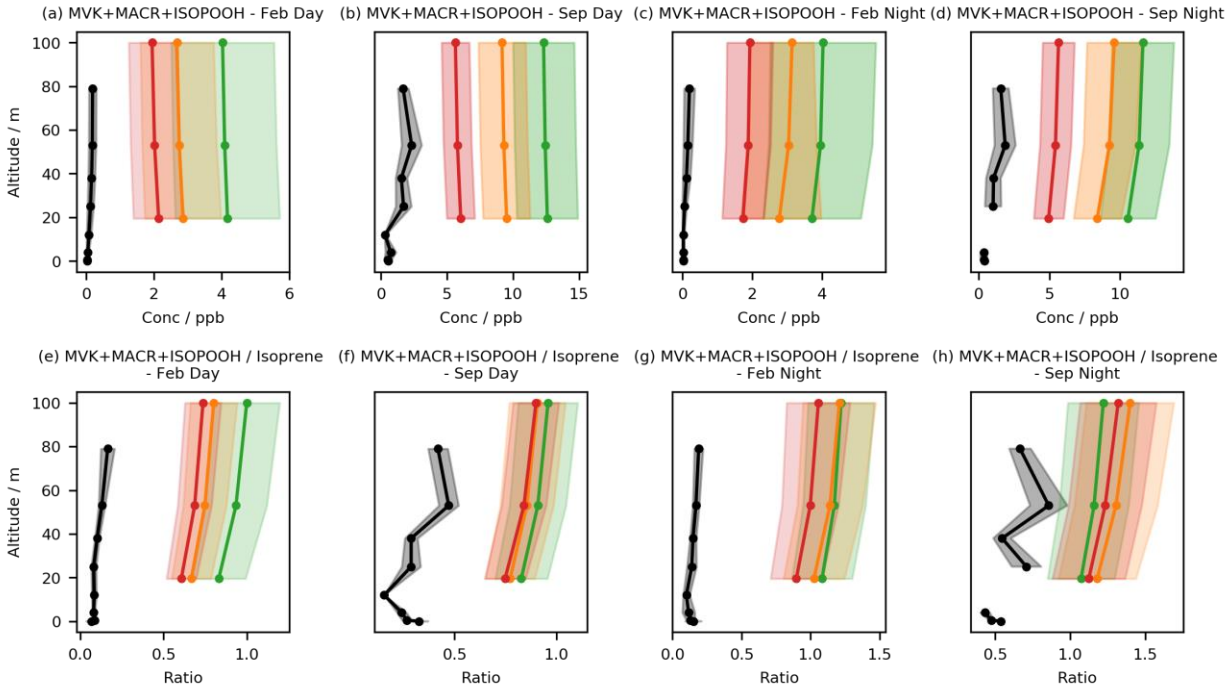

Figure S9 - Mean vertical profiles of the isoprene oxidation products MVK+MACR+ISOPOOH and the ratio of MVK+MACR+ISOPOOH to isoprene from observations taken at the ATTO tower (Yanez-Serrano et al., 2015) and model output from ST, CS and CS2. Daytime and nighttime periods are taken as 9:00-15:00 and 21:00-03:00 respectively. Shaded regions indicate ± 1 standard deviation from the mean.

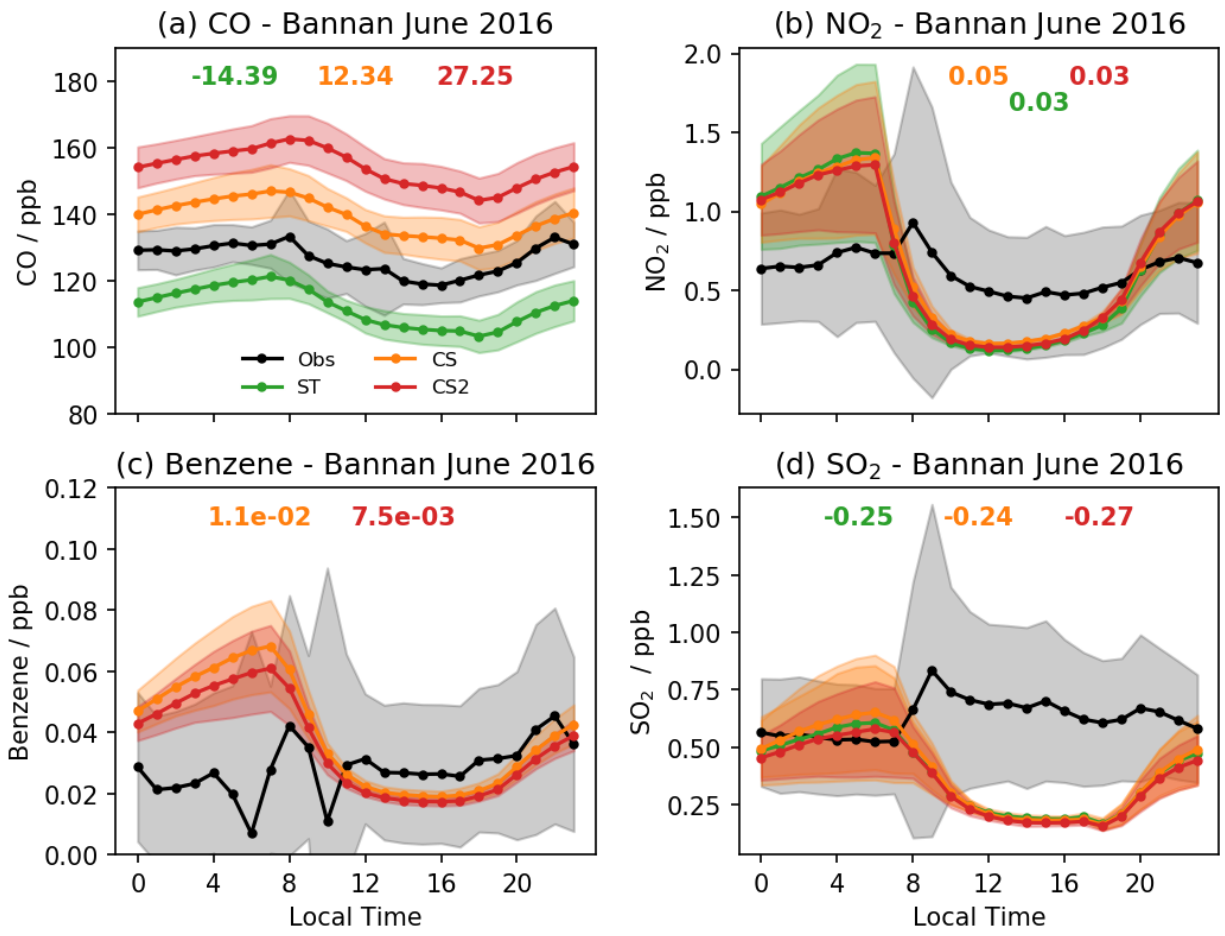

Figure S10 - Mean modelled (ST, CS and CS2) and observed diurnal profiles of CO, NO2, Benzene and SO2 from the Bannan site in the Amazon. Shading indicates ±1 standard deviation from the observation mean and the numbers in bold show the mean diurnal model bias (model - observations). (Note that the ST mechanism does include benzene as a species.).

939

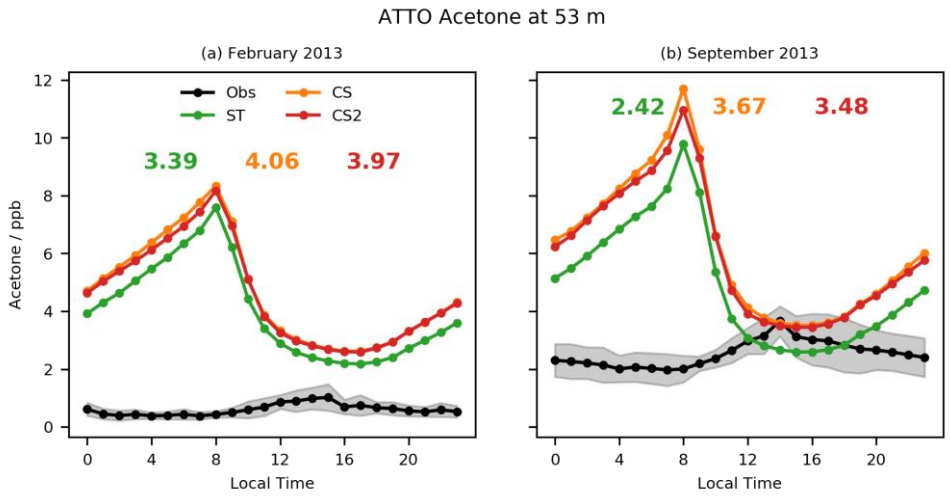

940

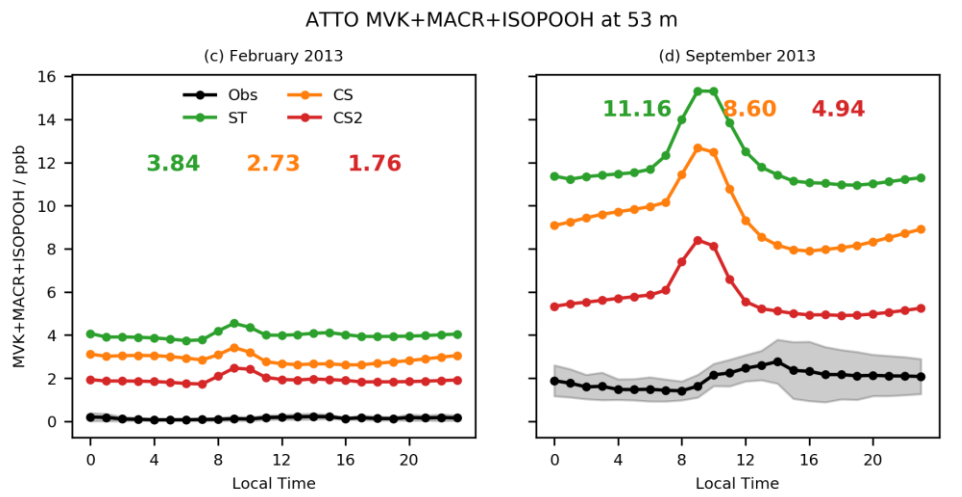

941

942

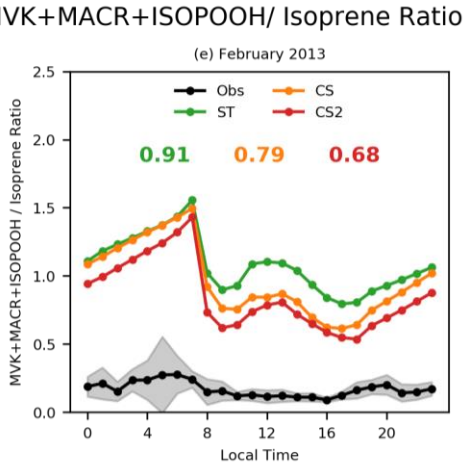

943

944

945

946

Figure S11. Mean modelled (ST, CS, CS2) and observed diurnal profiles of acetone, MVK+MACR+ISOPOOH at the ATTO tower. Observations are from the OP3 tower (e.g. Hewitt et al., 2010, Table 3) and model output from the most relevant grid cell. Shading indicates ±1 standard deviation from the observation mean and the numbers in bold show the mean diurnal model bias (model - observations).

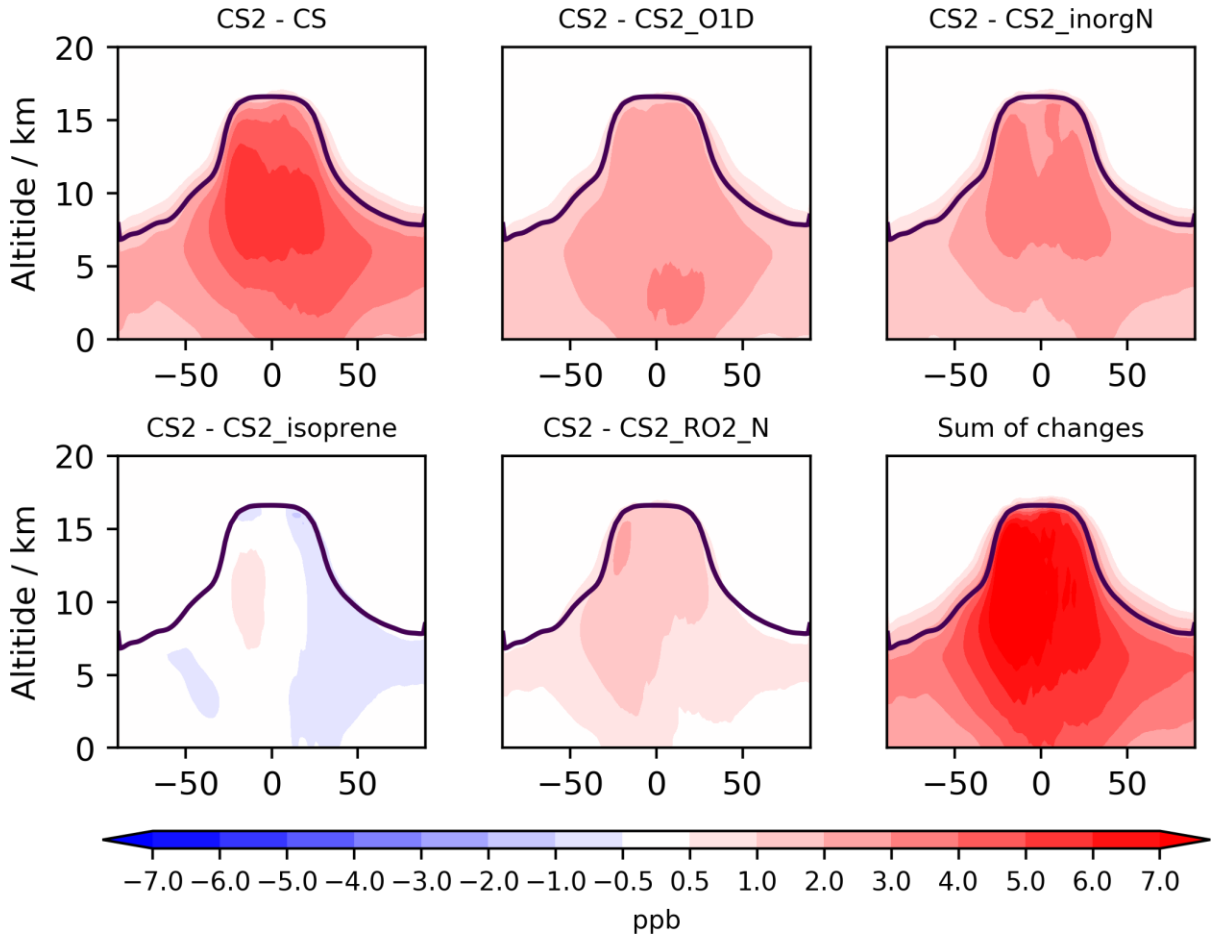

Figure S12. Zonal mean change in ozone mixing ratio for 2006 for CS2 and CS (top left), CS2 and the respective sensitivity tests and the sum of the changes from the sensitivity tests. The purple line shows the mean tropopause height.

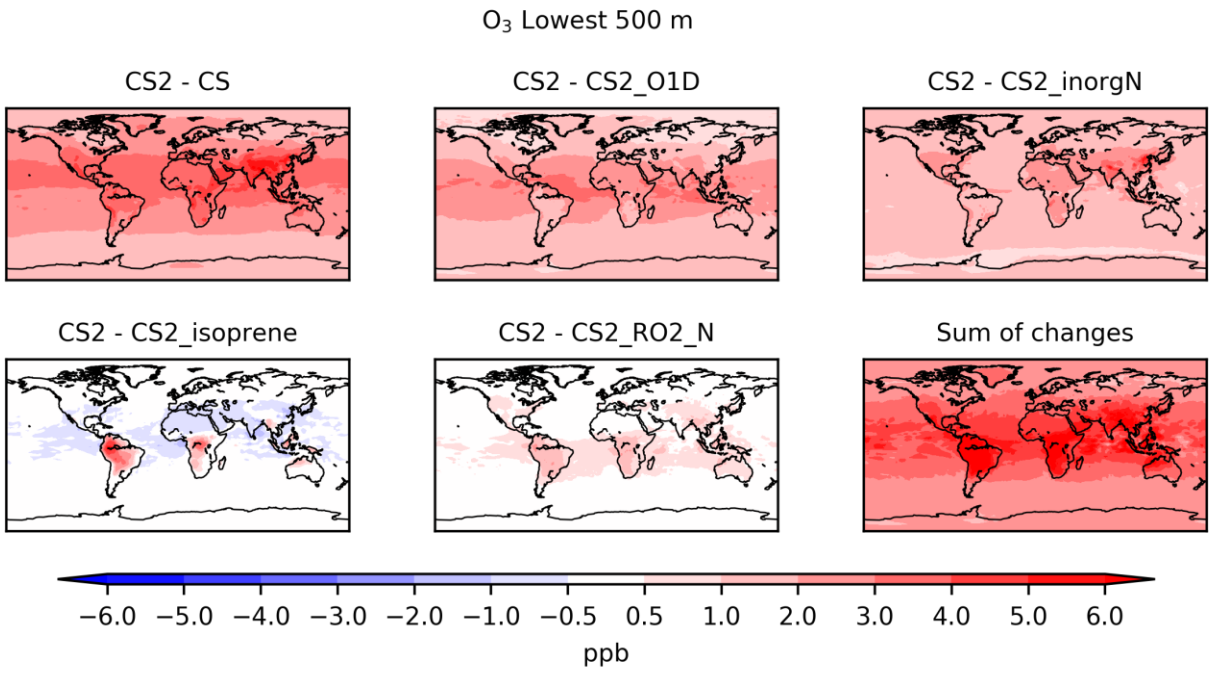

964
965
966 **Figure S13. Mean change in ozone mixing ratio for the lowest ~500 m for 2006 for CS2 and CS (top**
967 **left), CS2 and the respective sensitivity tests and the sum of the changes from the sensitivity tests.**
968
969

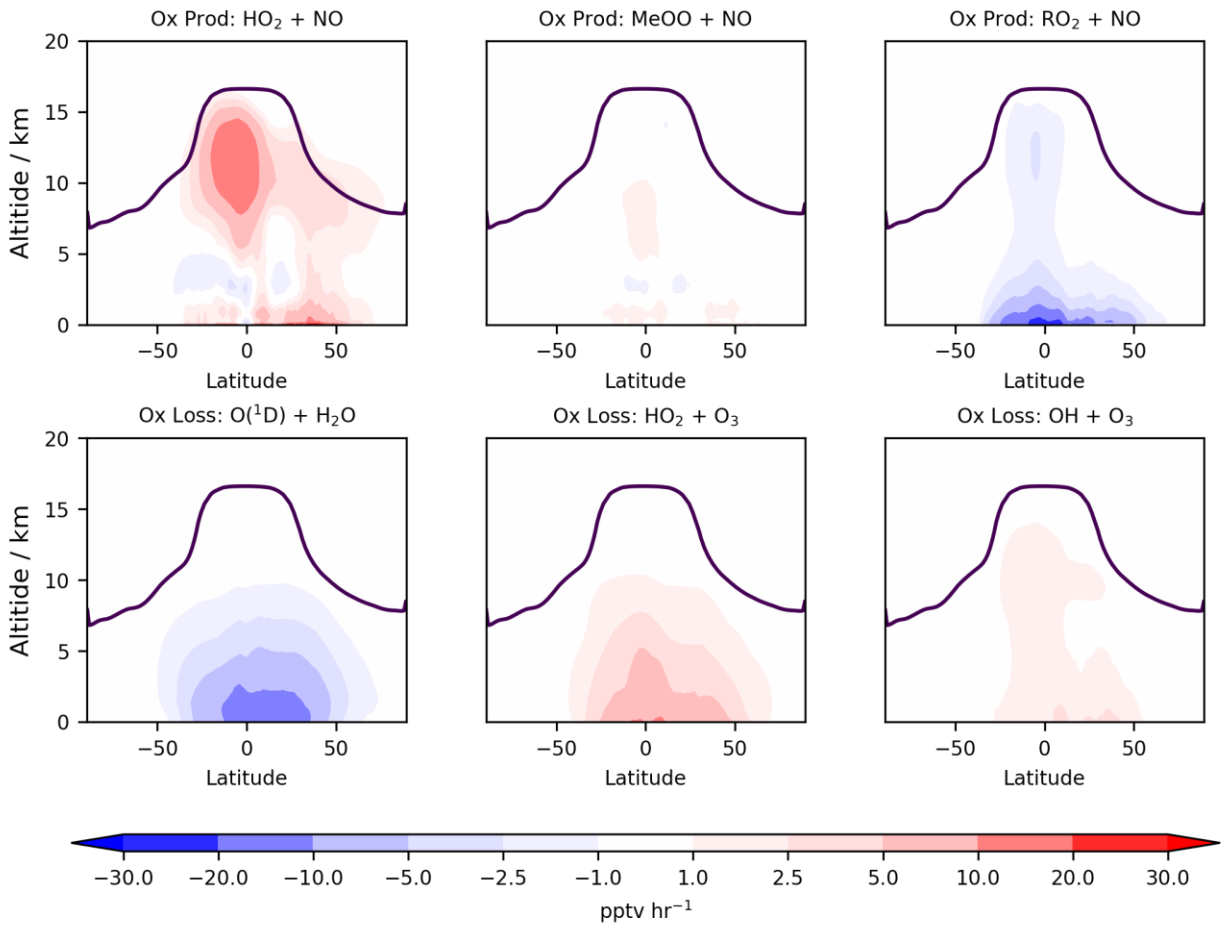

Figure S14. Tropospheric zonal mean change in the major production and loss Ox fluxes for CS2 - CS. These fluxes make up over 99%and 95% of total production and loss fluxes, respectively.

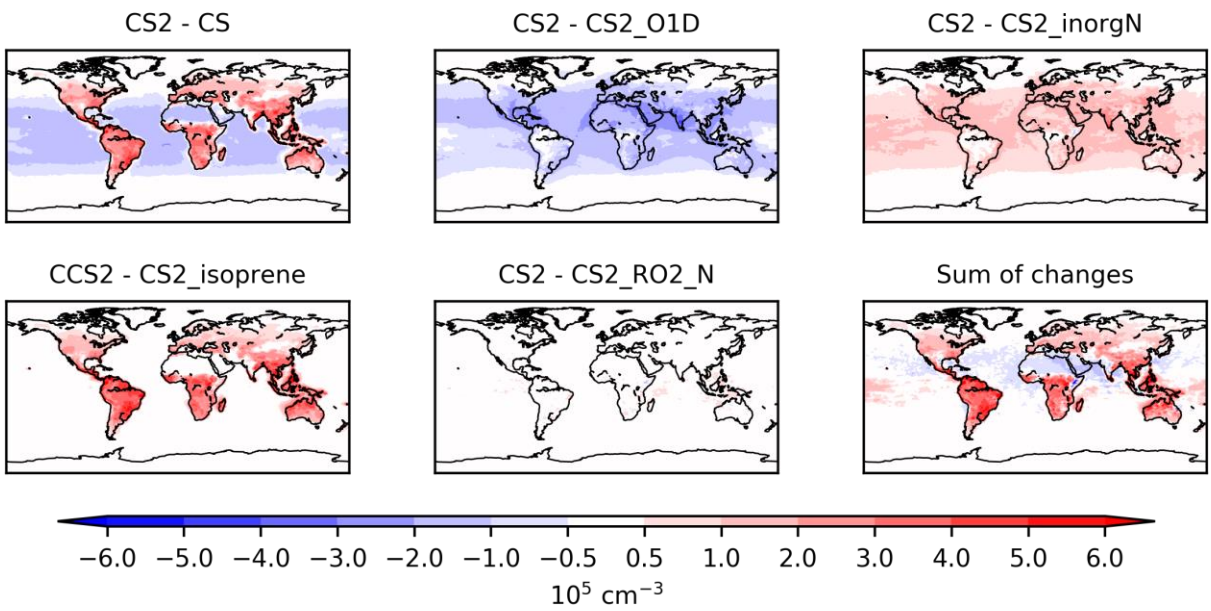

977
978

979 **Figure S15. Mean change in OH concentration for the lowest ~500 m for 2006 for CS2 and CS (top**
980 **left), CS2 and the respective sensitivity tests and the sum of the changes from the sensitivity tests.**

981
982
983
984
985

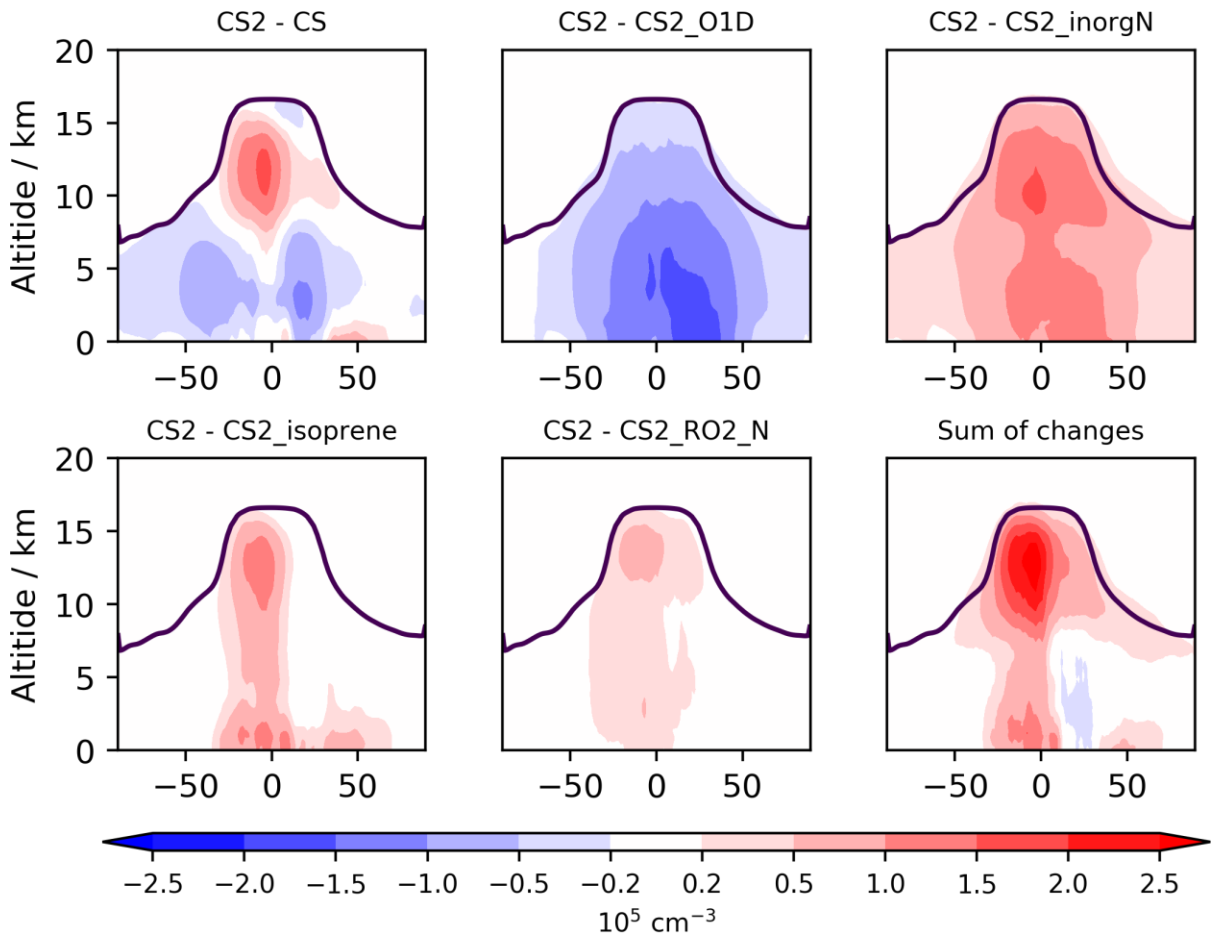

Figure S16. Tropospheric zonal mean change in OH for 2006 for CS2 and CS (top left), CS2 and the respective sensitivity tests and the sum of the changes from the sensitivity tests. The purple line shows the mean tropopause height.

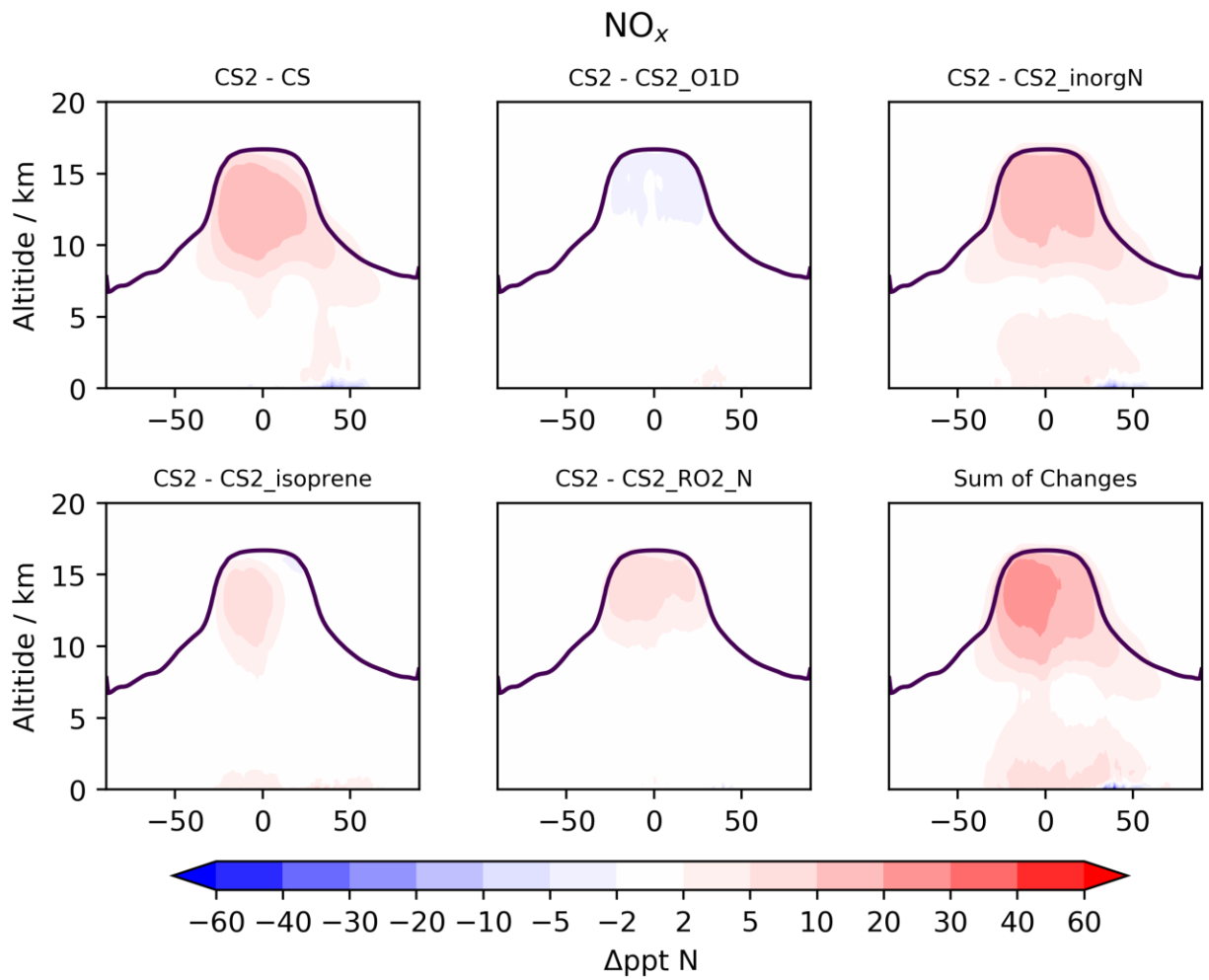

Figure S17. Zonal mean change in NOx for CS2 and CS (top left), CS2 and the respective sensitivity tests and the sum of the changes from the sensitivity tests. The purple line shows the mean tropopause height.

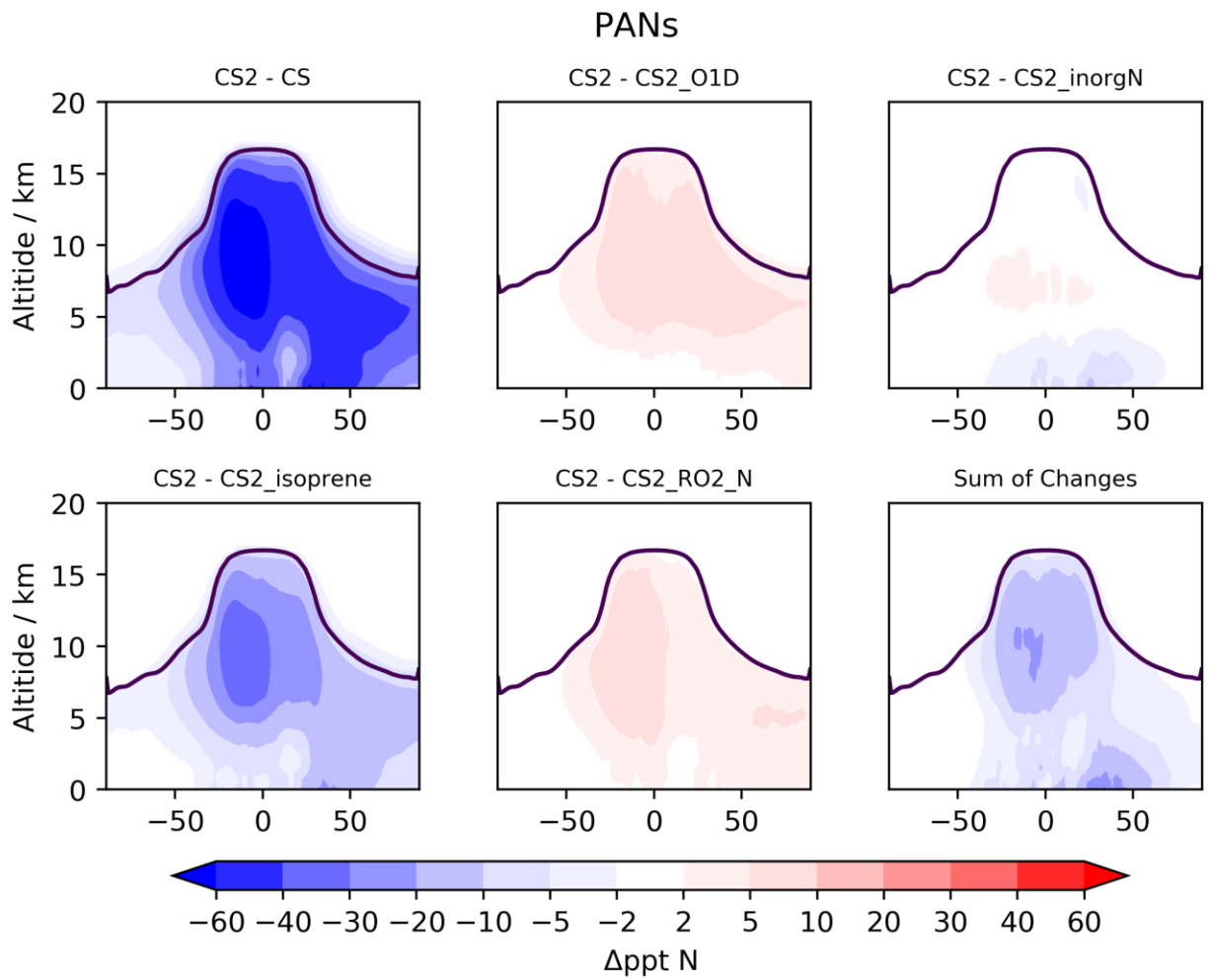

Figure S18. Tropospheric zonal mean change in PANs for CS2 and CS (top left), CS2 and the respective sensitivity tests and the sum of the changes from the sensitivity tests. The purple line shows the mean tropopause height.

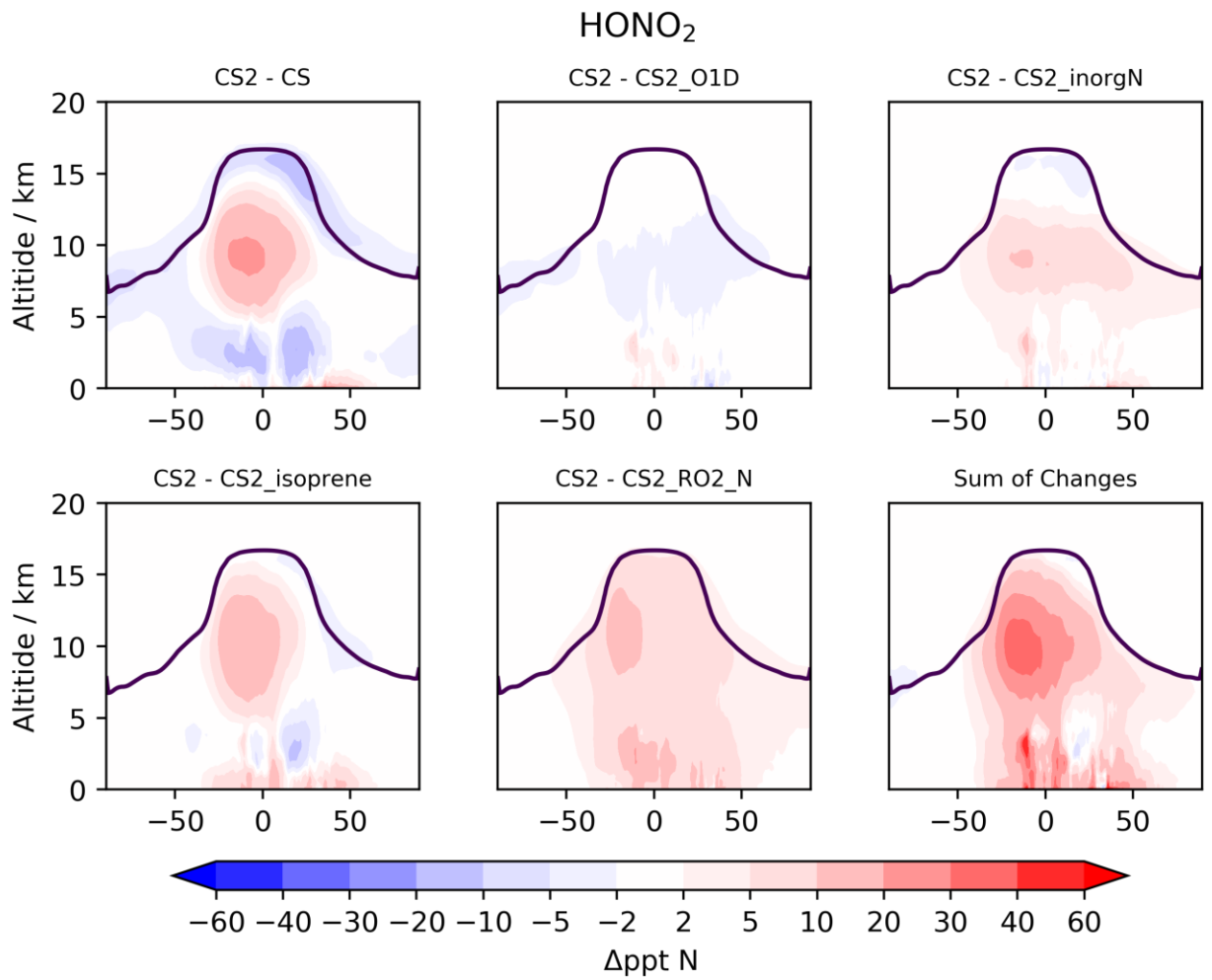

Figure S19. Zonal mean change in $HONO_2$ for CS2 and CS (top left), CS2 and the respective sensitivity tests and the sum of the changes from the sensitivity tests. The purple line shows the mean tropopause height.

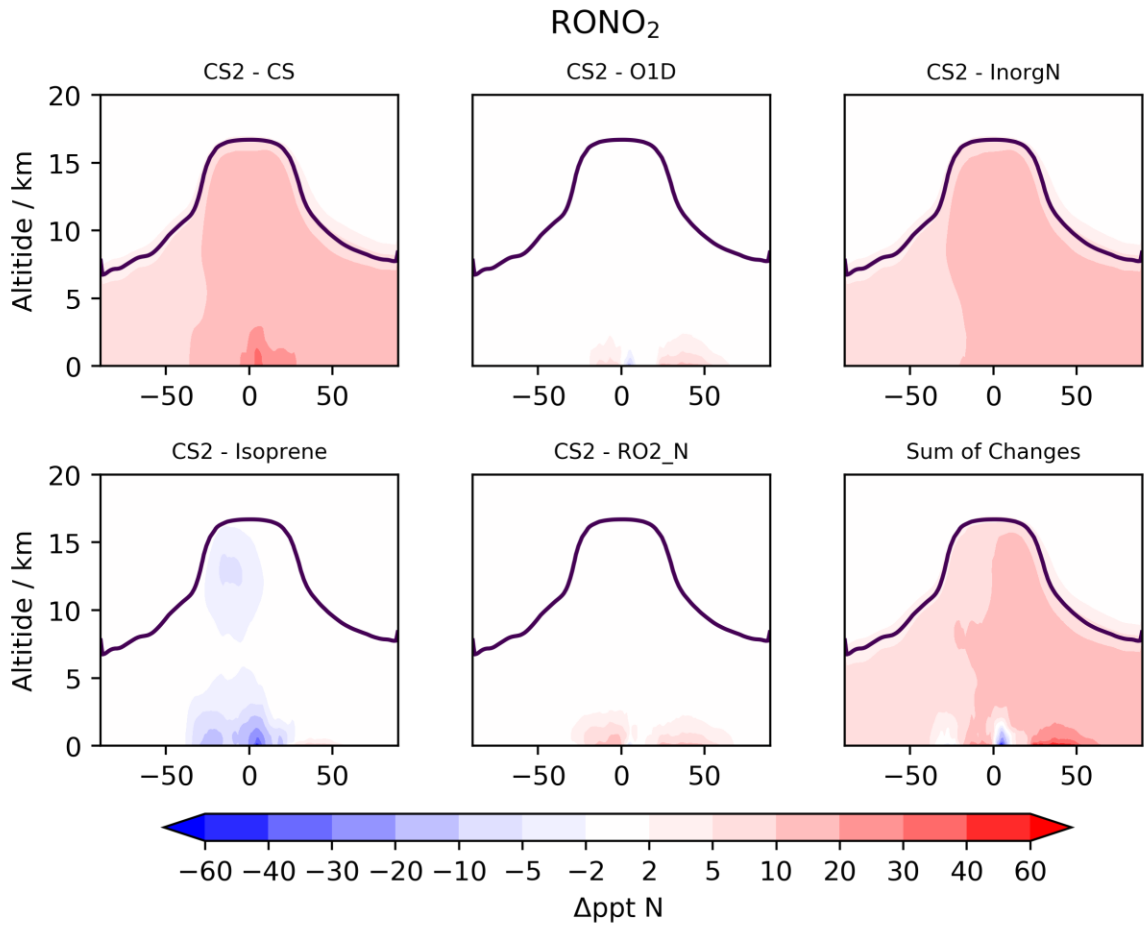

Figure S20. Zonal mean change in $RONO_2$ for CS2 and CS (top left), CS2 and the respective sensitivity tests and the sum of the changes from the sensitivity tests. The purple line shows the mean tropopause height.

Table S4 - Annual mean Ox diagnostics for CS, CS2 and sensitivity tests. Note that these data refer to the single year of analysis used for the sensitivity tests rather than the 4 year mean as in Table 4 so the absolute values for CS and CS2 may differ from Table 4.

	CS	**CS2**	**CRI_v2_2_O1D**	**CRI_v2_2_inorgN**	**CRI_v2_2_isoprene**	**CRI_v2_2_RO2_N**
O_3 Burden (Tg)	324	351	334	334	353	345
O_x Lifetime (days)	17.23	18.63	17.28	18.73	18.62	18.61
Chemical Production (Tg year^{-1})	**6579**	**6585**	**6780**	**6217**	**6650**	**6478**

HO_2 + NO	4100	4231	4347	4009	4200	4165
MeOO + NO	1575	1585	1659	1468	1565	1549
NO + RO_2	852	720	721	694	833	718
Other	51	49	52	47	52	46
Chemical Loss (Tg year^{-1})	**5837**	**5761**	**6003**	**5446**	**5828**	**5669**
$O(^1D)$ + H_2O	3168	2939	3221	2830	2956	2906
HO_2 + O_3	1659	1812	1760	1700	1814	1781
OH + O_3	739	796	809	711	785	772
O_3 + Alkene	167	101	94	100	162	99
Other	105	113	109	104	112	110
Deposition (Tg year^{-1})	**1129**	**1202**	**1155**	**1155**	**1200**	**1183**

Section S5

CO

The CO burden increased by 3.2% from 343 Tg in CS to 354 Tg in CS2 with gains of 4-5 ppb in the SH low altitudes and 2-4 ppb in much of the troposphere (Fig. 10). Tropospheric destruction of CO by OH increased by 3.2% (~100 Tg yr^{-1}) with increases of 5-10% in the tropical and midlatitude PBL driven by the enhanced oxidising capacity and greater CO production. However, this increased destruction was outweighed by a 4.4% increase in chemical production, driven primarily by the updates to the isoprene scheme, illustrated by the large column increases occurring over the regions with high BVOC emissions (Fig. S26).

Table S5 - Annual mean CO diagnostics for CS and CS2.

	CRI-STRAT	**CRI-STRAT 2**
CO burden / Tg	326.8	337.9

CO lifetime / days	38.1	38.3
Production / Tg CO year^{-1}	**3227.5**	**3326.7**
Emissions / Tg CO year^{-1}	1110.2	1110.7
HCHO + OH/NO_3 / Tg CO year^{-1}	589.3	555.3
HCHO + hv / Tg CO year^{-1}	1228.6	1239.4
Other Chemistry / Tg CO year^{-1}	86.2	179.7
Other Photolysis / Tg CO year^{-1}	213.1	242.2
Loss / Tg CO year^{-1}	**3158.2**	**3254.2**
CO + OH / Tg CO year^{-1}	2994.6	3086.6
CO Dry Dep / Tg CO year^{-1}	163.6	167.6
Net production / Tg CO year^{-1}	**69.3**	**72.5**

HCHO

The HCHO burden decreased by 10% in CS2 (1.20 Tg to 1.08 Tg), driven primarily by the change to isoprene chemistry with a small contribution from the increased HCHO photolysis flux. Added competition from ISOPO2 isomerisation leads to the production of methylglyoxal (CARB6) and hydroxy acetone (CARB7), at the expense of methacrolein and methyl vinyl ketone (lumped together as UCARB10). The former species tend to produce less HCHO than the latter, resulting in the greatest reduction in HCHO column over the regions with the greatest biogenic emissions (Fig. S26).

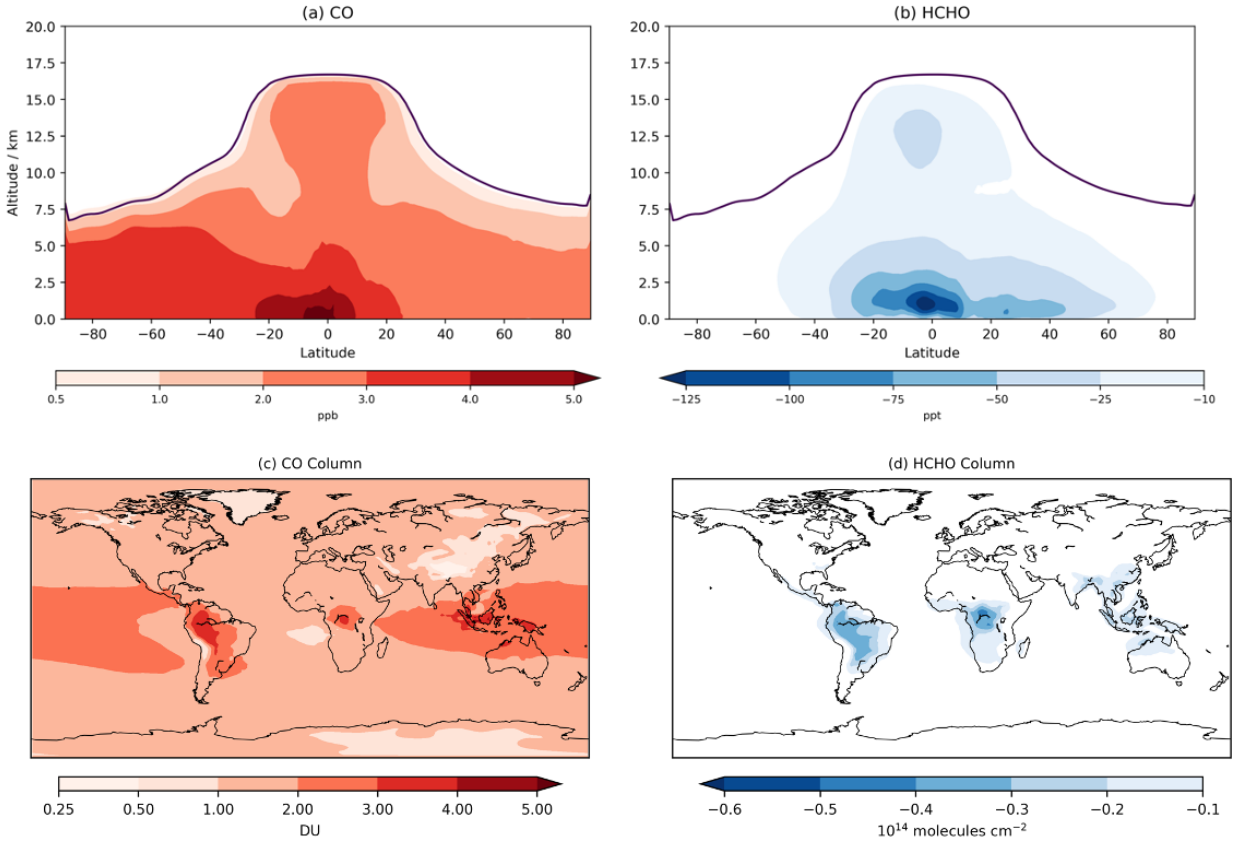

Figure S21. Annual zonal mean changes in (a) CO and (b) HCHO and annual column changes in (c) CO and (d) HCHO.

Section S6 Impact of Photolysis Changes

The CS2 mechanism featured the updates to photolysis described in section 2. To isolate the impacts of these changes on tropospheric ozone and OH, a further run was performed using the CS2 mechanism but with photolysis parameters from the CS mechanism. This run was run for 2 years with the 2nd year analysed and compared to the same year in the longer CS2 run.

The change in photolysis had produced minor changes in tropospheric oxidants. The tropospheric O_3 burden decreased by 0.09% (0.32 Tg). Changes in most of the troposphere were below 0.2 ppb (~1%), at least an order of magnitude lower than the simulated changes between CS and CS2 (with updated photolysis) while larger increases of 0.5-1.5 ppb (0.5-1%) were observed around the tropical tropopause (Fig. S27). Therefore, we can conclude the change in O_3 between CS and CS2 s being driven predominantly by the change in chemistry rather than photolysis.

Updating the photolysis increased the air mass-weighted OH concentration by 0.98% (1.0×10^4 cm^{-3}), compared to a decrease of 1.55% between in CS2 relative to CS. Spatially, OH increased in most of the troposphere by less than 2.0×10^4 cm^{-3} (0.2-0.5%) (Fig S28) with the largest absolute increases in at low altitude 40S-50N. By comparison, OH is simulated to decrease from CS to CS2 in the bulk of the

troposphere by at least 2.0 x 10^4 cm^{-3} and more than 5.0 x 10^4 cm^{-3} in tropical and midlatitudes (excluding the tropopause). Therefore, the update to the photolysis, by increasing OH in CS2, actually reduces the change in OH from CS to CS2 rather than being a cause of the mechanistic difference.

An important caveat to this is low altitude northern hemisphere midlatitude OH which increased from CS to CS2 and also from the base to updated photolysis setup. The impact on OH of the photolysis update must be compared to the impact of the changes to the chemistry, notably isoprene HOx recycling and changes to $O(^1D)$'s reaction pathways. Crucially, we see that the change in OH averaged over the lowest 500m from CS to CS2 is significantly larger than the change arising from the photolysis update, particularly over the regions with significant BVOC emissions such as the Amazon and other tropical regions (Fig. S28). That said, the impact of updated photolysis may be more significant over the parts of Europe and North America where the OH increase between CS and CS2 is smaller. Overall however we can conclude that the update to the photolysis is not a major driver of the significant changes to low altitude OH, rather the update in chemistry between CS and CS2 is the major driver.

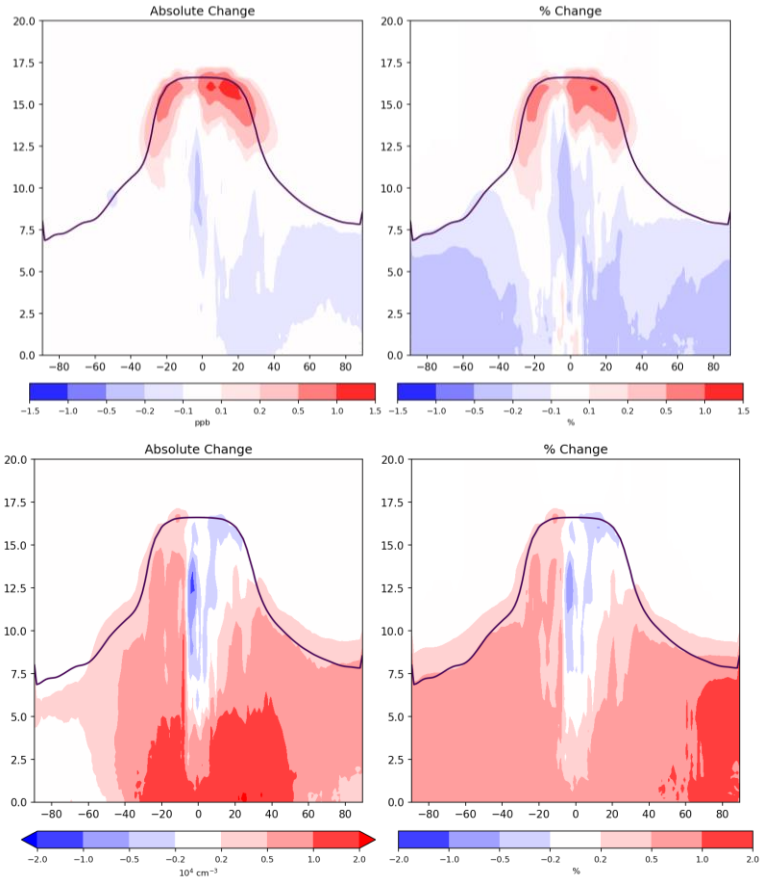

Figure S22. Zonal mean changes in O_3 (upper panels) and OH (lower panels) between CS2 and CRI_v2_2_photo. The purple line shows the mean tropopause height.

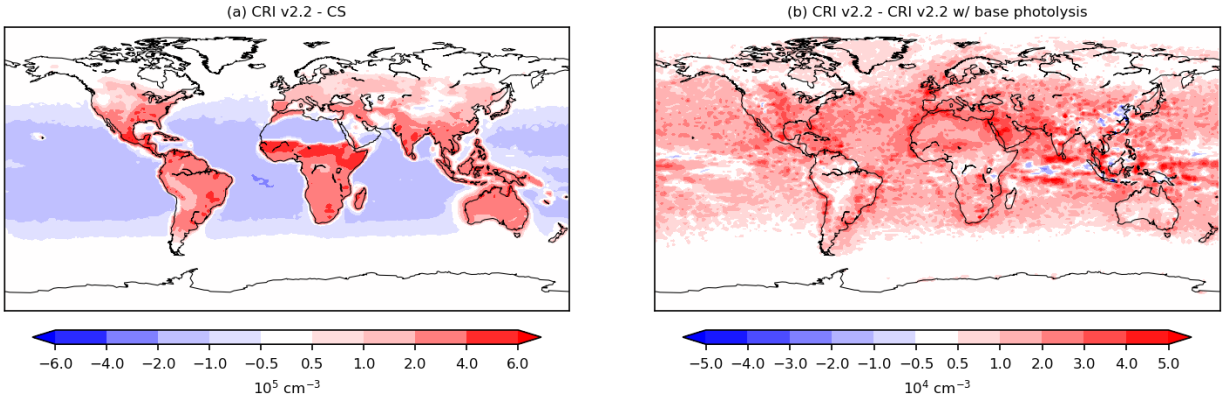

Figure S23. Change in OH averaged over lowest ~500m between (a) CS2 and CS and (b) CS2 and CRI_v2_2_photo. Note that the scale of (a) is an order of magnitude greater than (b).

References

Bondy, A., Craig, R., Zhang, Z., Gold, A., Surratt, J., Ault, A. (2017). Isoprene-Derived Organosulfates: Vibrational Mode Analysis by Raman Spectroscopy, Acidity-Dependent Spectral Modes, and Observation in Individual Atmospheric Particles Thermodynamic Model of the System H+−NH4+−SO42-−NO3-−H2O at Tropospheric Temperatures 122(1), 303 - 315.

Budisulistiorini, S. H., Li, X., Bairai, S. T., Renfro, J., Liu, Y., Liu, Y. J., McKinney, K. A., Martin, S. T., McNeill, V. F., Pye, H. O. T., Nenes, A., Neff, M. E., Stone, E. A., Mueller, S., Knote, C., Shaw, S. L., Zhang, Z., Gold, A., and Surratt, J. D.: Examining the effects of anthropogenic emissions on isoprene-derived secondary organic aerosol formation during the 2013 Southern Oxidant and Aerosol Study (SOAS) at the Look Rock, Tennessee ground site, Atmos. Chem. Phys., 15, 8871-8888, 10.5194/acp-15-8871-2015, 2015.

Lee, B. H., Lopez-Hilfiker, F. D., Mohr, C., Kurtén, T., Worsnop, D. R., and Thornton, J. A.: An Iodide-Adduct High-Resolution Time-of-Flight Chemical-Ionization Mass Spectrometer: Application to Atmospheric Inorganic and Organic Compounds, Environmental Science & Technology, 48, 6309-6317, 10.1021/es500362a, 2014

Zhang, Z., Lin, Y., Zhang, H., Surratt, J., Ball, L., Gold, A. (2012). Technical Note: Synthesis of isoprene atmospheric oxidation products: isomeric epoxydiols and the rearrangement products cis- and trans-3-methyl-3,4-dihydroxytetrahydrofuran Atmospheric Chemistry and Physics 12(18), 8529 - 8535.

B. H. Lee *et al.*, An iodide-adduct high-resolution time-of-flight chemical-ionization mass spectrometer: application to atmospheric inorganic and organic compounds. *Environmental Science & Technology* **48**, 6309-6317 (2014).

F. D. Lopez-Hilfiker *et al.*, A novel method for online analysis of gas and particle composition: description and evaluation of a Filter Inlet for Gases and AEROsols (FIGAERO). *Atmos. Meas. Tech.* **7**, 983-1001 (2014).

T. J. Bannan *et al.*, A method for extracting calibrated volatility information from the FIGAERO-HR-ToF-CIMS and its experimental application. *Atmospheric Measurement Techniques* **12**, 1429-1439 (2019).

M. Priestley *et al.*, Observations of Isocyanate, Amide, Nitrate, and Nitro Compounds From an Anthropogenic Biomass Burning Event Using a ToF-CIMS. *Journal of Geophysical Research: Atmospheres* **123**, 7687-7704 (2018).

Y. Liu *et al.*, Isoprene photochemistry over the Amazon rainforest. *Proceedings of the National Academy of*

Sciences **113**, 6125-6130 (2016).

M. Le Breton *et al.*, Online gas- and particle-phase measurements of organosulfates, organosulfonates and nitrooxy organosulfates in Beijing utilizing a FIGAERO ToF-CIMS. *Atmos. Chem. Phys.* **18**, 10355-10371 (2018).

T. J. Bannan *et al.*, The first UK measurements of nitryl chloride using a chemical ionization mass spectrometer in central London in the summer of 2012, and an investigation of the role of Cl atom oxidation. *Journal of Geophysical Research: Atmospheres* **120**, 5638-5657 (2015).

P. F. DeCarlo *et al.*, Field-Deployable, High-Resolution, Time-of-Flight Aerosol Mass Spectrometer. *Analytical Chemistry* **78**, 8281-8289 (2006).

S. S. de Sá *et al.*, Influence of urban pollution on the production of organic particulate matter from isoprene epoxydiols in central Amazonia. *Atmos. Chem. Phys.* **17**, 6611-6629 (2017).